JACS
JOURNAL OF THE AMERICAN CHEMICAL SOCIETY
Article
pubs.acs.org/JACS

Synthesis and Electronic Structure of Bis(imino)pyridine Iron Metallacyclic Intermediates in Iron-Catalyzed Cyclization Reactions

Jordan M. Hoyt,[†] Kevin T. Sylvester,[‡] Scott P. Semproni,[†] and Paul J. Chirik*,[†]

[†]Department of Chemistry, Princeton University, Princeton, New Jersey, United States 08544

[‡]Department of Chemistry and Chemical Biology, Baker Laboratory, Cornell University, Ithaca, New York, United States 14850

Supporting Information

ABSTRACT: The bis(imino)pyridine iron dinitrogen compound, ($^{iPr(TB)}$PDI)Fe(N_2)$_2$ ($^{iPr(TB)}$PDI = 2,6-(2,6-^{i}Pr$_2$-C_6H_3-N=C-$(CH_2)_3$)$_2$(C_5H_1N)) is an effective precatalyst for the [2π + 2π] cycloaddition of diallyl amines as well as the hydrogenative cyclization of N-tosylated enynes and diynes. Addition of stoichiometric quantities of amino-substituted enyne and diyne substrates to ($^{iPr(TB)}$PDI)Fe(N_2)$_2$ resulted in isolation of catalytically competent bis(imino)pyridine iron metallacycle intermediates. A combination of magnetochemistry, X-ray diffraction, and Mössbauer spectroscopic and computational studies established S = 1 iron compounds that are best described as intermediate-spin iron(III) (S_{Fe} = 3/2) antiferromagnetically coupled to a chelate radical anion (S_{PDI} = 1/2). Catalytically competent bis(imino)pyridine iron diene and metallacycles relevant to the [2π + 2π] cycloaddition were also isolated and structurally characterized. The combined magnetic, structural, spectroscopic, and computational data support an Fe(I)−Fe(III) catalytic cycle where the bis(imino)pyridine chelate remains in its one-electron reduced radical anion form. These studies revise a previous mechanistic proposal involving exclusively ferrous intermediates and highlight the importance of the redox-active bis(imino)pyridine chelate for enabling catalytic cyclization chemistry with iron.

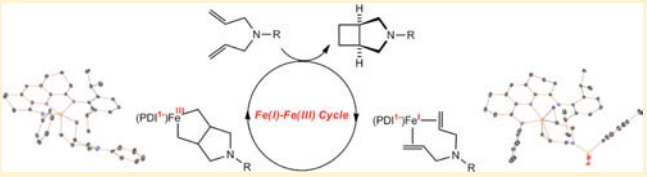

INTRODUCTION

Metal-catalyzed cyclization reactions that combine multiple π-fragments have emerged as a powerful, atom economical and often selective method for the synthesis of various hetero- and carbocycles encountered in target-directed synthesis.[1−7] Exemplary substrates include α,ω-dienes, enynes, and diynes that can participate in metal-catalyzed cycloisomerization[4] or undergo additional coupling with other unsaturates including CO, alkynes, olefins, and nitriles.[8−10] A pervasive mechanistic theme invokes coordination of two unsaturated moieties to a reduced metal center followed by oxidative coupling to form a metallacycle which enables the critical C−C bond-forming event and often dictates the chemo-, regio-, or even enantioselectivity of the overall transformation.[11−14] This metallacyclic intermediate is also susceptible to a range of organometallic transformations including hydrogenation, metal-mediated atom transfer, reductive elimination, β-hydrogen elimination, or various migratory insertion processes that can be used for further functionalization.[15−17] An alternative mechanistic pathway has also been identified and involves formation of metal allylic intermediates arising from alkene carbo- or hydrometalation and is frequently invoked in palladium-catalyzed transformations.[18−20]

The continued motivation to develop sustainable synthetic methods has renewed interest in the discovery of catalytic methods using earth-abundant elements in lieu of precious metals.[21−23] Due to its relatively low cost and high terrestrial abundance, catalysts based on iron have received considerable attention in cyclization catalysis.[22−25] Seminal studies by Takacs and co-workers demonstrated the utility of reduced iron compounds in formal [4π + 4π] ene-type reactions[26] as well as enediene carbocyclizations for the stereoselective formation of bicycles.[27] The latter has been applied to the enantioselective synthesis of (−)-protoemetinol and related alkaloids.[28] Simple iron salts such as $FeCl_3$[29] or $FeCl_2$ treated with excess ^{t}BuMgCl[30] have been reported to promote the cyclization of enynes. Fürstner and co-workers have described the rich catalytic chemistry associated with [Li(TMEDA)[(η^5-C_5H_5)Fe(C_2H_4)$_2$] including enyne and diyne skeletal rearrangements, [4π + 2π], [5π + 2π], [2π + 2π + 2π], and Alder-ene-type cyclizations.[31]

The bis(imino)pyridine iron dinitrogen complexes, (^{iPr}PDI)-Fe(N_2)$_2$[32] and [(^{Me}PDI)Fe(N_2)]$_2$(μ_2-N_2),[33] are highly active and often highly selective precatalysts for a range of transformations including olefin hydrogenation[34] and hydrosilylation.[35] For 1,6-enynes and diynes, hydrogenation with catalytic quantities of (^{iPr}PDI)Fe(N_2)$_2$ furnished the corresponding 3,4-disubstituted five-membered ring compounds with little evidence for linear hydrogenation products.[36] The turnover frequencies of the iron compounds are comparable to rhodium-catalyzed hydrogenative cyclization reactions pioneered by Krische and co-workers.[37−39] The iron-catalyzed reactions, unlike the rhodium variants, do not require exogeneous base implicating homo- rather than heterolytic H_2 splitting. Stoichiometric experiments and deuterium labeling

Received: January 26, 2013
Published: February 28, 2013

dx.doi.org/10.1021/ja400895j | J. Am. Chem. Soc. 2013, 135, 4862−4877

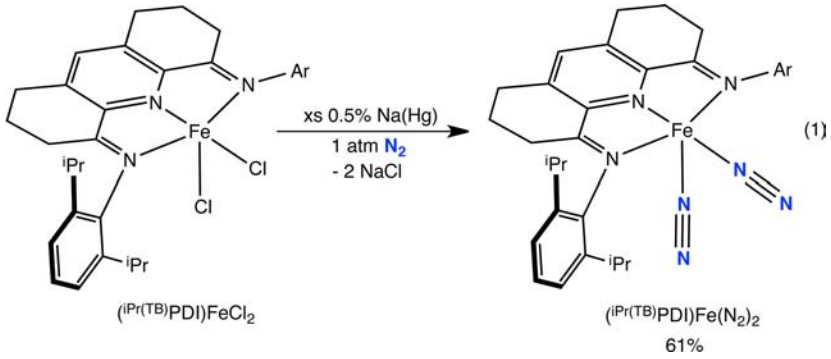

studies on cyclization reactions promoted by (^{iPr}PDI)Fe(N_2)$_2$ established cyclometalation of the isopropyl methyl substituents from an aryl substituent on the bis(imino)pyridine ligand as operative during catalytic turnover.[36]

In chemistry more unique to reduced bis(imino)pyridine iron compounds, (^{iPr}PDI)Fe(N_2)$_2$ promotes an intramolecular [2π + 2π] cycloaddition of α,ω-dienes to furnish the corresponding [3.2.0]bicycloheptanes in high yield.[40] An intermolecular variant of this reaction has also been discovered whereby both (^{iPr}PDI)Fe(N_2)$_2$ and [(^{Me}PDI)Fe(N_2)]$_2$(μ_2-N_2) serve as effective precatalysts for the [2π + 2π] cycloaddition of ethylene and butadiene to form vinylcyclobutane.[41] Notably, no cyclohexene, arising from thermally allowed [4π + 2π] Diels–Alder chemistry, was observed, highlighting the selectivity of the iron catalysts for cyclobutane formation. Examples of thermal, intramolecular [2π + 2π] cycloaddition have been reported previously but typically require activated π-systems such as allenes, allenenes, or alleynes to induce turnover.[42]

The ability of bis(imino)pyridine iron complexes to promote unique [2π + 2π] cycloaddition chemistry and compete with precious metals in hydrogenative cyclizations has inspired efforts to understand the mechanisms of these catalytic reactions. We were particularly interested in understanding the features of the bis(imino)pyridine iron compounds that enable cyclobutane formation. The redox-activity of the bis(imino)pyridine chelate,[43−46] the ability to engage in reversible electron transfer with the metal center,[47] raises the intriguing possibility that this feature of the iron catalyst enables the unique cycloaddition chemistry. In our initial communication[40] we postulated, on the basis of model compounds that were not catalytically competent, that the redox-activity of the bis(imino)pyridine chelate maintains iron(II) compounds throughout the catalytic cycle and prevents formation of iron(0) species that could be deleterious for catalyst stability.[48] Here we describe a new bis(imino)pyridine iron dinitrogen precatalyst for the intramolecular [2π + 2π] cycloaddition of α,ω-dienes as well as the hydrogenative cyclization of enynes and diynes. For each type of catalytic cyclization reaction, a catalytically competent iron metallacycle has been isolated and the electronic structure established by a combination of X-ray diffraction, spectroscopic, and computational studies. Based on these findings, new mechanistic insights on iron-catalyzed cyclizations and the role of the redox-active bis(imino)pyridine chelate have been elucidated.

RESULTS AND DISCUSSION

Synthesis of Bis(imino)pyridine Iron Dinitrogen Complex Bearing a Tetrahydroacridyl Ligand. Our studies commenced with the synthesis of a new bis(imino)-pyridine iron dinitrogen complex. Previous studies from our laboratory have shown that C−C reductive elimination from a formally 18-electron, bis(imino)pyridine iron allyl alkyl compound is induced by strong field ligands such as carbon monoxide and 1,3-butadiene,[41] suggesting that imine dissociation may be operative during catalytic turnover. To experimentally explore this possibility, a bis(imino)pyridine variant was targeted where the imine backbones are tethered to the meta-position of the pyridine ring. This approach was inspired by Goldberg's study probing chelate opening prior to C−C reductive elimination from six-coordinate platinum(IV) complexes.[49]

The requisite bis(imino)pyridine iron dichloride precursor, ($^{iPr(TB)}$PDI)$FeCl_2$ ($^{iPr(TB)}$PDI = 2,6-(2,6-$^{i}Pr_2$-C_6H_3-N=C-$(CH_2)_3$)$_2$(C_5H_1N)) was previously reported by Kim and coworkers.[50] Sodium amalgam reduction of ($^{iPr(TB)}$PDI)$FeCl_2$ with excess 0.5% sodium amalgam under a dinitrogen atmosphere followed by filtration and recrystallization furnished a dark green solid identified as ($^{iPr(TB)}$PDI)Fe(N_2)$_2$ in 61% isolated yield (eq 1).

Diamagnetic ($^{iPr(TB)}$PDI)Fe(N_2)$_2$ was characterized by ^{1}H NMR, infrared, and zero-field ^{57}Fe Mössbauer spectroscopies. The solid-state structure was determined by single crystal X-ray diffraction, and a representation of the molecular structure is presented in Figure 1. Selected bond distances and angles are reported in Table 1 as well as the corresponding metrical parameters for (^{iPr}PDI)Fe(N_2)$_2$ for comparison. The overall molecular geometry of ($^{iPr(TB)}$PDI)Fe(N_2)$_2$ is best described as

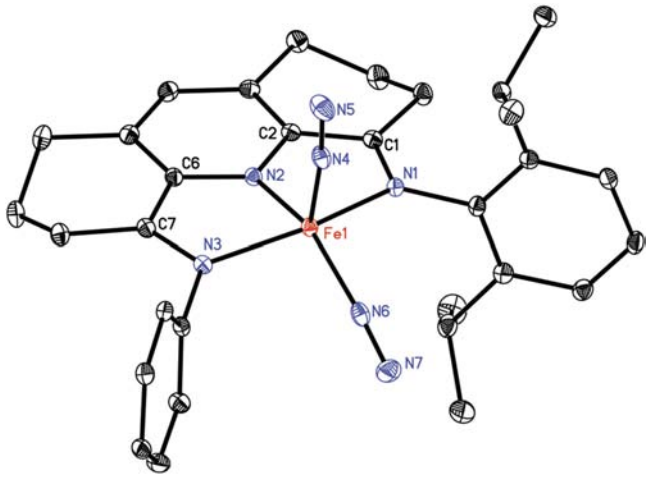

Figure 1. Solid-state structure for ($^{iPr(TB)}$PDI)Fe(N_2)$_2$ at 30% ellipsoids. Isopropyl substituents on one aryl ring and hydrogen atoms omitted for clarity.

dx.doi.org/10.1021/ja400895j | J. Am. Chem. Soc. 2013, 135, 4862−4877

Table 1. Selected Bond Distances (Å) and Angles (deg) for ($^{iPr(TB)}$PDI)Fe(N_2)$_2$ and (^{iPr}PDI)Fe(N_2)$_2$[a]

	($^{iPr(TB)}$PDI)Fe(N_2)$_2$	(^{iPr}PDI)Fe(N_2)$_2$
Fe(1)−N(1)	1.986(2)	1.947(2)
Fe(1)−N(2)	1.828(2)	1.836(1)
Fe(1)−N(3)	1.982(2)	1.945(2)
Fe(1)−N(4)	1.860(2)	1.880(2)
Fe(1)−N(6)	1.833(2)	1.834(1)
N(1)−C(1)	1.332(3)	1.334(2)
N(3)−C(7)	1.330(3)	1.333(2)
N(2)−C(2)	1.369(3)	1.377(2)
N(2)−C(6)	1.364(2)	1.379(2)
C(1)−C(2)	1.414(2)	1.427(2)
C(6)−C(7)	1.418(3)	1.428(3)
N(1)−Fe(1)−N(2)	79.58(7)	79.90(7)
N(1)−Fe(1)−N(3)	156.30(7)	154.77(7)
N(2)−Fe(1)−N(6)	150.77(8)	159.09(8)
N(4)−Fe(1)−N(6)	102.70(8)	98.02(8)
N(3)−C(7)−C(6)	113.4(2)	112.6(2)
N(1)−C(1)−C(2)	113.3(2)	113.5(2)

[a]The data for (^{iPr}PDI)Fe(N_2)$_2$ are taken from ref 32.

square pyramidal with the bis(imino)pyridine chelate and one of the dinitrogen ligands defining the basal plane. As reported by Kim and co-workers,[50] the rigidity of the chelate backbone opens the iron coordination sphere and results in elongated iron−imine bonds. In ($^{iPr(TB)}$PDI)Fe(N_2)$_2$, the Fe−N_{imine} bonds are 1.986(2) and 1.982(2) Å and are longer than the values of 1.947(2) and 1.945(2) Å in (^{iPr}PDI)Fe(N_2)$_2$. The N_{imine}−C_{imine} distances are elongated to 1.332(3) and 1.330(3) Å and the C_{imine}−C_{ipso} distances contracted to 1.414(2) and 1.418(3) Å, consistent with a redox noninnocent, π-accepting chelate as established for (^{iPr}PDI)Fe(N_2)$_2$.[51,52]

The solution behavior of ($^{iPr(TB)}$PDI)Fe(N_2)$_2$ was investigated by infrared spectroscopy, as previous studies have established an equilbrium between four- and five-coordinate bis(imino)pyridine iron dinitrogen complexes with each possessing a distinct electronic structure.[51] In pentane solution, three bands were observed. Two, centered at 2124 and 2061 cm^{-1}, are assigned to ($^{iPr(TB)}$PDI)Fe(N_2)$_2$ and are more reduced than the values of 2132 and 2073 cm^{-1} reported for (^{iPr}PDI)Fe(N_2)$_2$. A single band was also located at 2025 cm^{-1} and assigned to the four-coordinate compound, ($^{iPr(TB)}$PDI)-FeN_2. This value is also significantly reduced from the band observed at 2046 cm^{-1} reported for (^{iPr}PDI)FeN_2, consistent with a more electron-donating ligand upon introduction of alkyl groups used to tether the imine groups to the central pyridine ring.

The electronic structure of ($^{iPr(TB)}$PDI)Fe(N_2)$_2$ was also studied by zero-field ^{57}Fe Mössbauer spectroscopy at 80 K. A doublet was observed in the solid state, consistent with exclusive isolation of the five-coordinate complex, ($^{iPr(TB)}$PDI)-Fe(N_2)$_2$. The isomer shift of 0.45 mm/s is slightly higher than the value of 0.39 mm/s reported for (^{iPr}PDI)Fe(N_2)$_2$ (Table 2), consistent with the elongated iron−imine bonds observed in the solid-state structure. Full molecule, density functional theory calculations were also performed, and a restricted Kohn−Sham (RKS) solution successfully reproduced the experimentally observed Mössbauer parameters (δ = 0.38 mm/s; ΔE_Q = 0.75 mm/s), consistent with a covalent iron compound that is adquately described as a resonance hybrid between Fe(0) and Fe(II) canonical forms.[51]

Table 2. Zero-Field ^{57}Fe Mössbauer Spectroscopic Parameters for Bis(imino)pyridine Iron Compounds Relevant to This Study[a]

compound	δ (mm/s)	ΔE_Q (mm/s)[b]
($^{iPr(TB)}$PDI)Fe(N_2)$_2$	0.45	0.83
RKS	*0.38*	*0.75*
(^{iPr}PDI)Fe(N_2)$_2$	0.39	−0.53
(^{iPr}PDI)FeN_2	0.38	+1.72[c,f]
(^{iPr}PDI)Fe(biphenyl)	0.07	+3.58[d]
(^{Me}PDI)Fe(biphenyl)	0.05	3.69
1	0.17	3.05
BS(3,1)[e]	*0.15*	*+2.59*
(^{iPr}PDI)Fe(diyne-**C**)	0.22	2.79
2	0.23	2.22
BS(3,1)[e]	*0.16*	*+2.16*
(^{iPr}PDI)Fe(enyne-**D**)	0.27	2.65
3	0.63	2.47
BS(3,1)[e]	*0.65*	*+2.20*
4	0.30	2.66
BS(3,1)[e]	*0.24*	*+2.38*
5	0.30	2.58
6	0.73	1.81
BS(3,1)[e]	*0.83*	*+1.47*
7	0.62	2.58

[a]Data were collected at 80 K, and values reported in italics are computed values. [b]Unless a sign is reported, all values of ΔE_Q are absolute values. [c]Values taken from refs 51 and 53. [d]Values taken from ref 54. [e]Broken symmetry solution resulting where the iron−imine distances are fixed based on the values obtained from the experimentally determined crystal structures. Computed values from geometry-optimized solutions where an imine ligand has undergone dissociation are reported in the Supporting Information. [f]Sign determined by applied field measurement.

Evaluation of Catalytic Competency. With a new bis(imino)pyridine iron dinitrogen complex in hand, we explored its catalytic performance in intramolecular [2π + 2π] cycloaddition as well as hydrogenative enyne and diyne cyclization. Stirring a 0.10 M benzene-d_6 solution of either diallyl-*tert*-butylamine or diallylaniline with 10 mol % of ($^{iPr(TB)}$PDI)Fe(N_2)$_2$ resulted in rapid cyclization, furnishing the corresponding azobicyclo[3.2.0]heptane in near quantitative yield (Scheme 1). For these substrates, the activity of ($^{iPr(TB)}$PDI)Fe(N_2)$_2$ is similar but slightly reduced as compared to the previously reported (^{iPr}PDI)Fe(N_2)$_2$ precatalyst.[40] Although relatively high iron loadings of 10 mol % were used for initial catalyst screening, effective turnover was achieved at reduced catalyst concentrations of 1 mol %.

($^{iPr(TB)}$PDI)Fe(N_2)$_2$ also proved to be an effective precatalyst for the hydrogenative cyclization of both enynes and diynes. Exposure of an 0.14 M benzene-d_6 solution of *N*-allyl-*N*-(but-2-ynyl)-4-methylbenzenesulfonamide (**A**) to 4 atm of H_2 in the presence of 10 mol % of ($^{iPr(TB)}$PDI)Fe(N_2)$_2$ furnished a mixture of saturated and unsaturated pyrrolidines (Scheme 1). At shorter reaction times (30 min), the unsaturated pyrrolidine predominates, constituting 81% of the product mixture, with the balance of the material being the saturated heterocycle. The saturated compound arises from hydrogenation of the unsaturated pyrrolidine and was observed as a 52:48 mixture of syn and anti diastereomers. Continuing the hydrogenation for 3 h resulted in exclusive formation of the saturated product with no change in the diastereoselectivity.

dx.doi.org/10.1021/ja400895j | J. Am. Chem. Soc. 2013, 135, 4862−4877

Scheme 1. Iron-Catalyzed [2π + 2π] and Hydrogenative Cyclization Reactions Promoted by ($^{iPr(TB)}$PDI)Fe(N_2)$_2$

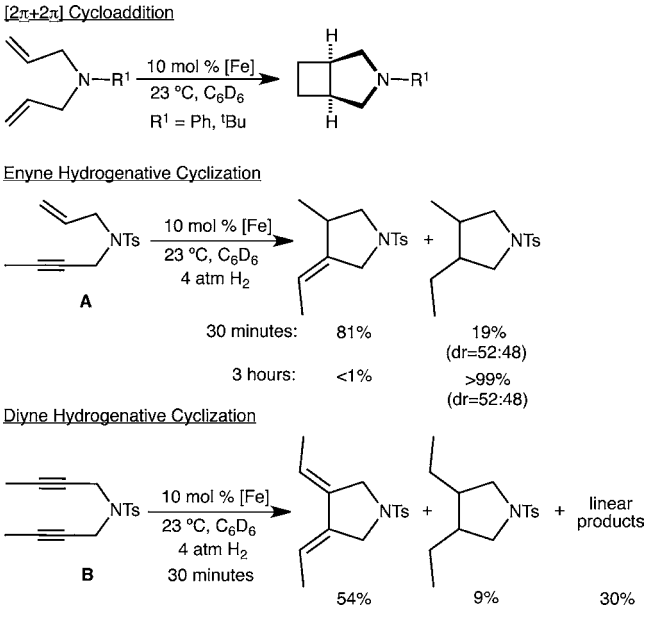

The hydrogenative cyclization of *N*,*N*-dibut-2-ynyl-4-methylbenzenesulfonamide (**B**) was accomplished under the same conditions as the catalytic enyne chemistry (Scheme 1) and yielded 54% of the 3,4-dialkenyl pyrrolidine as the (*E*,*E*) isomer after 30 min. At this time interval, 9% of the saturated pyrrolidine was observed along with 30% of linear products arising from hydrogenation of the alkyne without cyclization. The linear products are a mixture of amino-alkenes and alkanes. Formation of such a quantity of linear products is a consequence of the increased hydrogenation activity of ($^{iPr(TB)}$PDI)Fe(N_2)$_2$ relative to (^{iPr}PDI)Fe(N_2)$_2$. For the latter iron precatalyst, almost exclusive cyclization was observed. The catalytic chemistry summarized in Scheme 1 clearly establishes the competency of ($^{iPr(TB)}$PDI)Fe(N_2)$_2$ in established iron-catalyzed cyclization reactions.

Synthesis and Electronic Structure of Bis(imino)-pyridine Iron Metallacycles: Hydrogenative Diyne and Enyne Cyclization. To isolate, characterize, and understand the electronic structure of catalytically relevant iron metallacycles, diyne substrates were initially explored. Our laboratory has recently reported the synthesis and characterization of iron metallacycles resulting from the C−C oxidative addition of biphenylene to (^{iPr}PDI)Fe(N_2)$_2$ and [(^{Me}PDI)Fe(N_2)]$_2$(μ_2-N_2).[54] Both (PDI)Fe(biphenyl) derivatives were determined to be iron(III) compounds with bis(imino)pyridine radical anions. Magnetic studies along with X-ray absorption and emission spectroscopies established spin crossover behavior from low to intermediate-spin ferric as a function of temperature. Although (^{iPr}PDI)Fe(biphenyl) was kinetically unstable to transfer dehydrogenation from an isopropyl aryl substituent, isolation of these compounds suggested that iron metallacycles related to diyne cyclization may also be possible.

Addition of a hexane solution of **B** to a hexane slurry of ($^{iPr(TB)}$PDI)Fe(N_2)$_2$ at 23 °C resulted in precipitation of a red solid identified as the desired iron metallacyclopentadiene, **1** in 84% yield (eq 2). The benzene-d_6 ^{1}H NMR spectrum of **1** at 23 °C was featureless and not useful for characterization of the compound. Similar spectroscopic properties were observed for (^{iPr}PDI)Fe(biphenyl).[54] A solid sample of **1** was analyzed by zero-field ^{57}Fe Mössbauer spectroscopy and exhibited a quadrupole doublet with an isomer shift of 0.17 mm/s and a quadrupole splitting (ΔE_Q) of 3.05 mm/s. Parameters in this range are consistent with an iron(III) compound but are by no means exclusive for this oxidation state assignment.[55] As reported in Table 2 however, the Mössbauer parameters for **1** are similar to those reported for both (^{iPr}PDI)Fe(biphenyl) and (^{Me}PDI)Fe(biphenyl).

The magnetic ground state of **1** was determined in both solution and the solid state. In benzene-d_6 at 23 °C a moment of 2.8 μB was determined by the method of Evans,[56] consistent with the spin only value for two unpaired electrons and an $S = 1$ molecule. Because (^{iPr}PDI)Fe(biphenyl) and (^{Me}PDI)Fe-(biphenyl) exhibit spin crossover, the solid-state magnetic susceptibility of **1** was measured by SQUID magnetometry from 2 to 300 K (Figure S2, Supporting Information). The data revealed simple paramagnetic behavior with no evidence for SCO. The magnetic moment plateaued at 3.0 μ_B, consistent with the solution measurements and an $S = 1$ ground state.

Single crystals of **1** were obtained from a concentrated diethyl ether solution stored at −35 °C. A representation of the solid-state molecular structure is presented in Figure 2. Selected bond distances and angles for all iron metallacycles structurally characterized in this work are presented in Table 3. The crystallographic data were a three-component twin that was successfully modeled and confirmed the identity of **1** as the metallacyclopentadiene. One molecule of diethyl ether was also present in the unit cell. The geometry about the metal can be described as distorted square pyramidal with one of the carbon substituents occupying the apical position. The C(39)−C(40) distance of 1.420(7) Å is diagnostic of C−C bond formation and the C(38)−C(39) and C(40)−C(41) bond lengths of 1.357(7) and 1.360(5) Å are as expected for a metallacyclopentadiene.

As is well established for redox-active bis(imino)-pyridines,[45,46] distortions to the bond distances of the chelate signal participation in the electronic structure of the compound

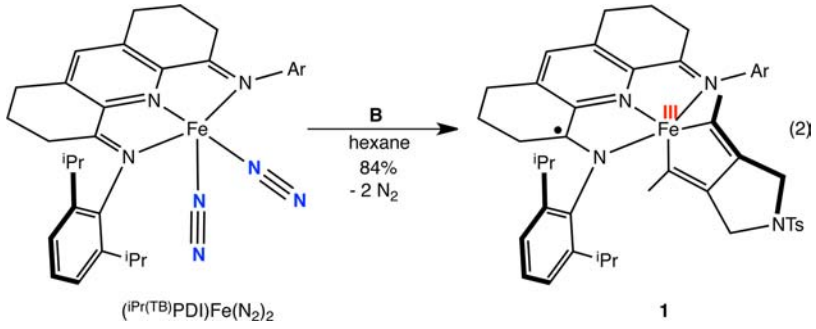

dx.doi.org/10.1021/ja400895j | J. Am. Chem. Soc. 2013, 135, 4862−4877

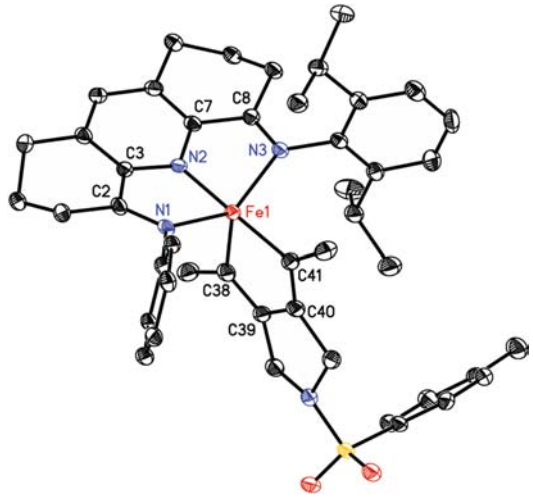

Figure 2. Solid-state structure for **1** at 30% ellipsoids. Isopropyl substituents on one aryl ring and hydrogen atoms omitted for clarity.

Table 3. Selected Bond Distances (Å) and Angles (deg) for 1−4

	1	2	3	4
Fe(1)−N(1)	2.073(2)	2.044(2)	2.738(2)	2.079(3)
Fe(1)−N(2)	1.862(5)	1.906(2)	2.012(2)	1.910(3)
Fe(1)−N(3)	2.069(4)	2.066(2)	2.040(2)	2.123(3)
Fe(1)−C(38)	2.004(5)	2.002(2)	2.092(2)	2.046(4)
Fe(1)−C(41)	1.996(6)	2.027(2)	2.090(2)	2.012(4)
N(1)−C(2)	1.327(7)	1.328(3)	1.286(3)	1.320(5)
N(3)−C(8)	1.327(8)	1.325(3)	1.321(3)	1.319(5)
C(2)−C(3)	1.424(6)	1.421(4)	1.470(3)	1.429(6)
C(7)−C(8)	1.421(7)	1.420(3)	1.431(3)	1.435(6)
C(38)−C(39)	1.357(7)	1.320(4)	1.394(3)	1.528(6)
C(39)−C(40)	1.420(7)	1.504(3)	2.778(2)	1.544(6)
C(40)−C(41)	1.360(5)	1.548(3)	1.397(3)	1.530(6)
N(1)−Fe(1)−N(2)	78.5(2)	77.57(7)	68.31(6)	77.5(1)
N(1)−Fe(1)−N(3)	143.4(1)	143.40(7)	148.84(6)	144.2(1)
N(2)−Fe(1)−N(3)	78.0(2)	77.45(7)	80.54(7)	77.5(1)
C(38)−Fe(1)−C(41)	85.3(2)	84.81(9)	150.67(8)	84.8(2)
C(38)−Fe(1)−N(1)	103.9(2)	105.38(8)	82.49(7)	106.6(1)
C(38)−Fe(1)−N(2)	96.4(2)	105.08(8)	98.09(8)	105.8(1)
C(38)−Fe(1)−N(3)	106.2(2)	106.66(8)	103.45(8)	104.6(1)
C(41)−Fe(1)−N(1)	100.8(2)	99.20(8)	83.91(7)	98.1(1)
C(41)−Fe(1)−N(2)	178.3(2)	170.07(7)	100.81(7)	169.2(2)
C(41)−Fe(1)−N(3)	101.9(2)	100.83(8)	101.64(7)	101.9(1)

and possible radical character. The elongation of the N_{imine}−C_{imine} bonds in **1** to 1.327(7) and 1.327(8) Å and the contraction of the C_{imine}−C_{ipso} distances to 1.424(6) and 1.421(7) Å are consistent with the established values for one electron reduction. The iron−imine bond lengths of 2.073(2) and 2.069(4) Å are also relatively long, a result of the constrained geometry imparted by tethering the imine carbon to the meta position of the pyridine ring. The metrical data from the solid-state structure of **1** in combination with magnetochemistry and the Mössbauer parameters clearly establish an overall S = 1 compound derived from an intermediate-spin ferrous center antiferromagneticaly coupled to a bis(imino)pyridine radical anion. Compound **1** is structurally similar to (^{iPr}PDI)Fe(biphenyl) with the exception of elongated Fe−N_{imine} (2.073(2) and 2.069(4) Å as compared to 1.959(2) and 1.988(2) Å) and Fe−C bond lengths (2.004(5) and 1.996(6) Å as compared to 1.965(3) and 1.943(3) Å) likely due to the more open bis(imino)pyridine chelate and the fully populated S = 1 state at the temperature of the X-ray data collection.

Full molecule DFT studies were also conducted using the ORCA program with the B3LYP functional.[57] This approach has proven successful for the electronic structure determination of other redox-active bis(imino)pyridine iron and cobalt complexes.[46,51,53,54,58−60] Geometry optimizations with **1** resulted in dissociation of the iron−imine bonds so the Fe−N_{imine} distances were constrained to the experimentally determined distances and the remainder of the molecule optimized. Subsequent calculations were performed in a similar manner. Bond distances and relative energies for all calculations can be found in the Supporting Information (Table S7). Unrestricted Kohn−Sham (UKS) calculations were performed for the S = 1 ground state along with various broken symmetry possibilities. In broken symmetry notation, BS(m,n) describes a state where there are m unpaired spin up electrons and n unpaired spin down electrons on separate fragments.[61−63] All S = 1 inputs converge to the same BS(3,1) solution, which emerged as the lowest energy of all of the computational solutions examined. The computed Mössbauer parameters (δ = 0.21 mm/s, ΔE_Q = +3.05 mm/s) from the BS(3,1) output successfully reproduce the experimental values (Table 2). A qualitative molecular orbital diagram and corresponding spin density plot for this solution are presented in Figure 3. This solution corresponds to an intermediate-spin Fe(III) center antiferromagnetically coupled to a bis(imino)pyridine radical anion, consistent with all of the experimental data. The two SOMOs accounting for the S = 1 state are almost exclusively metal based, corresponding to d_{z2} and d_{xz} orbitals on iron.

To determine if **1** was catalytically competent, the hydrogenative cyclization of substrate **B** was studied. Exposure of a benzene-d_6 solution of 0.14 M **B** and 10 mol % **1** to 4 atm H_2, identical conditions to those used with ($^{iPr(TB)}$PDI)Fe(N_2)$_2$, resulted in >98% conversion to products after 30 min at 23 °C.

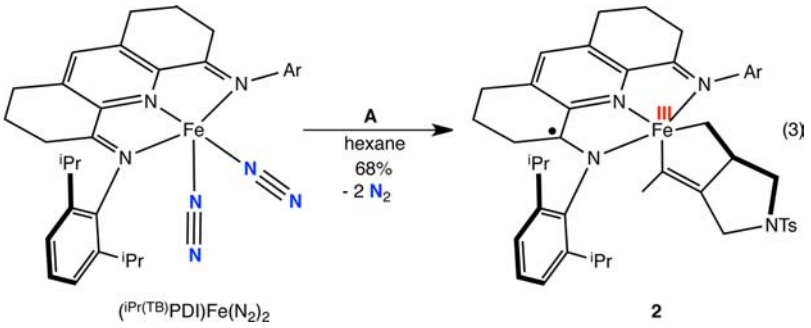

($^{iPr(TB)}$PDI)Fe(N_2)$_2$ **2**

dx.doi.org/10.1021/ja400895j | J. Am. Chem. Soc. 2013, 135, 4862−4877

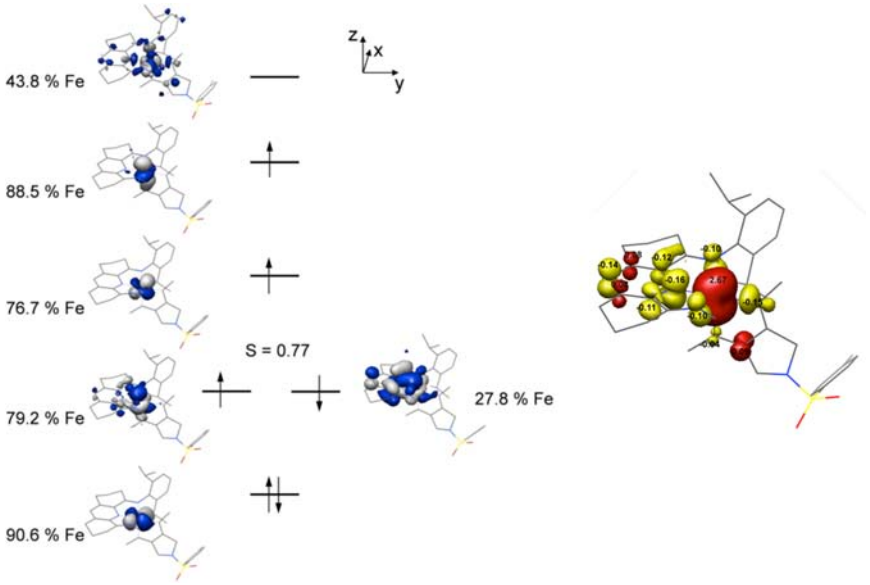

Figure 3. Qualitative molecular orbital diagram (left) and spin density plot (right) for the BS(3,1) solution for **1**.

As with ($^{iPr(TB)}$PDI)Fe(N_2)$_2$, 50% of the product mixture was the (*E*,*E*)-isomer of the 3,4-dialkenyl pyrrolidine with the remainder of the material identified as the saturated 3,4-diethyl pyrrolidine (10%) and open chain olefin isomerization and alkane products (32%) (Scheme 1). Thus, **1** is catalytically competent and a likely intermediate in iron-catalyzed diyne hydrogenative cyclization with no detectable change in activity or selectivity from the iron dinitrogen precursor.

The successful isolation and electronic structure determination of **1** prompted synthesis of bis(imino)pyridine iron metallacycles relevant to the hydrogenative cyclization of enynes. In our initial communication, we reported observation of the iron metallacycle resulting from addition of enyne **A** to (^{iPr}PDI)Fe(N_2)$_2$.[36] Because the metallacycle underwent transfer dehydrogenation with isopropyl aryl substituents and was therefore kinetically unstable, characterization data was limited to solution magnetochemistry and NMR spectroscopy. No structural or Mössbauer data were obtained, prohibiting definitive assignment of metal and ligand oxidation state. With ($^{iPr(TB)}$PDI)Fe(N_2)$_2$, addition of a hexane solution of *N*,*N*-dibut-2-ynyl-4-methylbenzenesulfonamide (**A**) to a hexane slurry of the iron dinitrogen compound furnished a red solid identified as the bis(imino)pyridine iron metallacycle **2** in 68% yield (eq 3).

Unlike **1**, the benzene-d_6 ^{1}H NMR spectrum of **2** at 23 °C exhibits 27 paramagnetically shifted resonances as anticipated for a C_s symmetric iron complex. A solution magnetic moment (Evans) of 2.8 μ_B was measured in benzene-d_6 at 23 °C, consistent with two unpaired electrons and an overall S = 1 ground state. The zero-field ^{57}Fe Mössbauer spectrum of **2** was recorded at 80 K and exhibits a quadrupole doublet with an isomer shift of 0.23 mm/s and a quadrupole splitting of 2.22 mm/s. The isomer shift for **2** is similar to **1** and is consistent with a similar iron oxidation state.

The molecular structure of **2** was also determined by single crystal X-ray diffraction (Figure 4). Minor positional disorder was present in the backbone of the ligand and in the metallacyclopentene that was successfully modeled. Selected bond distances and angles are reported in Table 3. As with **1**, an idealized square pyramidal iron complex was observed with the

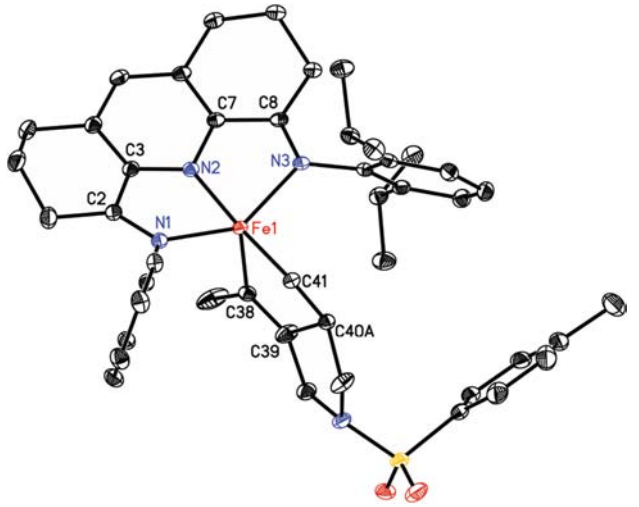

Figure 4. Solid-state structure for **2** at 30% ellipsoids. Hydrogen atoms and isopropyl substituents on one aryl ring omitted for clarity.

methylated carbon, C(38) defining the apical position. The C(39)−C(40) distance of 1.504(3) Å confirms C−C bond formation. The C(38)−C(39) distance of 1.320(4) Å is consistent with an alkene while the C(40)−C(41) bond length is extended to 1.548(3) Å, signaling a carbon−carbon single bond. The metrical parameters of the metallacycle are consistent with formation of an iron cyclopentene. The bond distances of the bis(imino)pyridine chelate are statistically indistinguishable from those in **1** and are consistent with one-electron reduction.[43,45,46] Thus, the metrical data, in combination with the Mössbauer parameters and magnetic measurements support an intermediate-spin ferric compound antiferromagnetically coupled to a bis(imino)pyridine radical anion.

Full molecule, broken symmetry DFT calculations (B3LYP) were performed on **2** and produced a similar BS(3,1) solution as for **1**. A qualitative molecular orbital diagram and a spin density plot for this solution are presented in Figure 5. The computed Mössbauer parameters (δ = 0.12 mm/s, ΔE_Q = 2.08 mm/s) are in good agreement with the experimental values

dx.doi.org/10.1021/ja400895j | *J. Am. Chem. Soc.* 2013, 135, 4862−4877

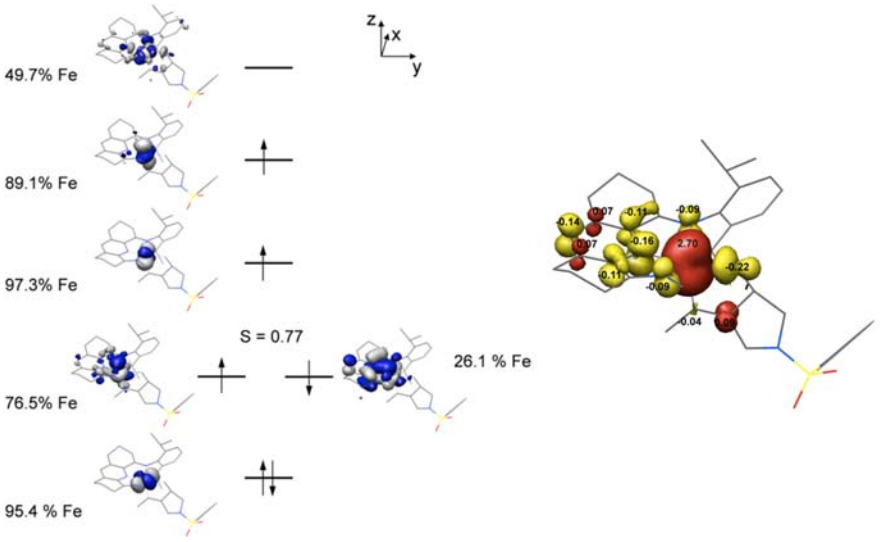

Figure 5. Qualitative molecular orbital diagram (left) and spin density plot (right) for the BS(3,1) solution for **2**.

(Table 2). The SOMOs, as with **1**, are iron-based with the unpaired electrons residing in principally d_{xz} and d_{z2} orbitals. The combined magnetic, spectroscopic, metrical, and computational data clearly establish **2** as an intermediate-spin Fe(III) compound antiferromagnetically coupled to a bis(imino)pyridine radical anion.

The successful isolation and characterization of **1** and **2** prompted reinvestigation of metallacycle synthesis with the original bis(imino)pyridine iron dinitrogen precatalyst, (^{iPr}PDI)Fe(N_2)$_2$ (Scheme 2). Specifically, we sought to employ

Scheme 2. Synthesis of [(^{iPr}PDI)Fe] Metallacycles Relevant to Diyne and Enyne Hydrogenative Cyclization

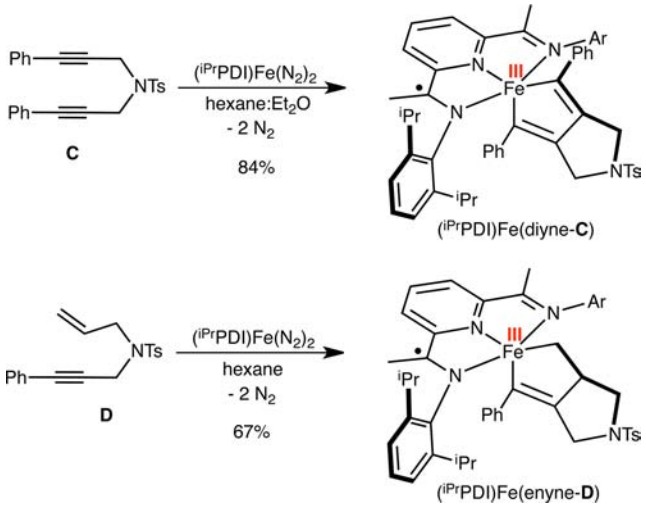

the precipitation strategy that proved successful with ($^{iPr(TB)}$PDI)Fe(N_2)$_2$. Accordingly, diyne **C** and enyne **D** with phenyl substituents were chosen to reduce the solubility of the resulting iron metallacycle in hydrocarbon solvents thereby facilitating isolation and potentially inhibiting deleterious transfer hydrogenation chemistry. Addition of 1 equiv of diyne **C** or enyne **D** to a hexane solution of (^{iPr}PDI)Fe(N_2)$_2$ resulted in precipitation of dark purple solids identified as the iron metallacycles, (^{iPr}PDI)Fe(diyne-**C**) or (^{iPr}PDI)Fe(enyne-**D**) in 84 and 67% yields, respectively (Scheme 2). Magnetic susceptibility measurements on both compounds were consistent with $S = 1$ molecules, in agreement with the ground states of **1** and **2**. In addition, the ^{57}Fe Mössbauer parameters (Table 2) for both (^{iPr}PDI)Fe(diyne-**C**) and (^{iPr}PDI)Fe(enyne-**D**) are similar to the analogous metallacycles with the tetrahydroacridyl-substituted bis(imino)pyridine iron complexes. Thus, all of the spectroscopic data support identical electronic structures between iron metallacycles with two different bis(imino)pyridine ligands.

Synthesis and Electronic Structure of Bis(imino)-pyridine Iron Metallacycles: [2π + 2π] Cycloadditions. The relative insolubility of enyne and diyne metallacycles derived from ($^{iPr(TB)}$PDI)Fe(N_2)$_2$ motivated exploration of the putative intermediates from a [2π + 2π] α,ω-diene cycloaddition. To complete the series, a hexane slurry of ($^{iPr(TB)}$PDI)Fe(N_2)$_2$ was treated with a hexane solution of diallyl tosyl amine and furnished a paramagnetic red solid, **3** (eq 4).

Single crystals of **3** were obtained from a hexane solution cooled to −35 °C, and X-ray diffraction established the identity of the compound not as the iron metallacyclopentane but rather the diolefin complex. The backbone methylene groups were disordered (~75:25) over two positions as was the iron center (90:10). Both disorders were successfully modeled and one orientation of each is presented in the depiction of the structure in Figure 6. The C(39)−C(40) distance of 2.778(2) Å is longer than those observed in **1** and **2**. Accordingly, the C(40)−C(41)/C(38)−C(39) distances of 1.394(3) and 1.397(3) Å are consistent with coordinated alkenes. Notably, the Fe(1)−N(1) distance of 2.738 Å is outside the range of a typical iron−imine dative bond and indicates dissociation of one arm of the chelate. Formation of a κ^2-bis(imino)pyridine ligand complicates correlation of the bond length distortions to the redox activity and ultimately metal and ligand oxidation state. As expected, for the portion of the ligand dissociated from the metal, N_{imine}−C_{imine} distance of 1.286(3) Å along with the C_{imine}−C_{ipso} bond length of 1.470(3) are hallmark values for a chelate in its neutral form. However, the portion of the ligand bound to the metal center demonstrates bond lengths, N_{imine}−C_{imine} distance of 1.321(3) Å and C_{imine}−C_{ipso} bond length of 1.431(3), that are indicative of a monoreduced chelate in both the bis(imino)pyridine and mono(imino)pyridine complexes.[64]

dx.doi.org/10.1021/ja400895j | J. Am. Chem. Soc. 2013, 135, 4862−4877

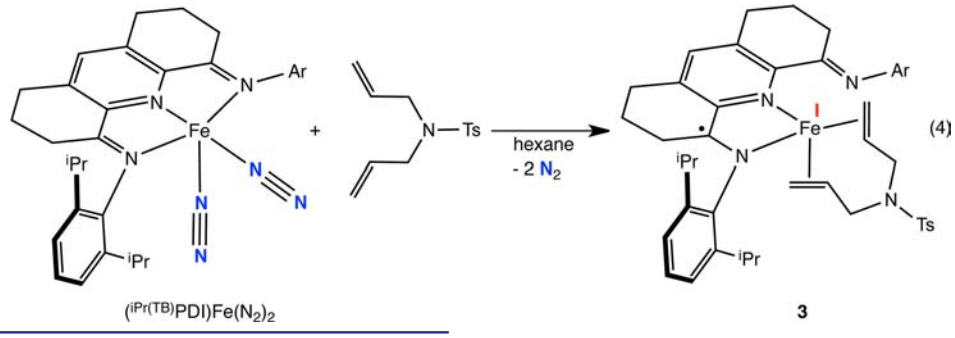

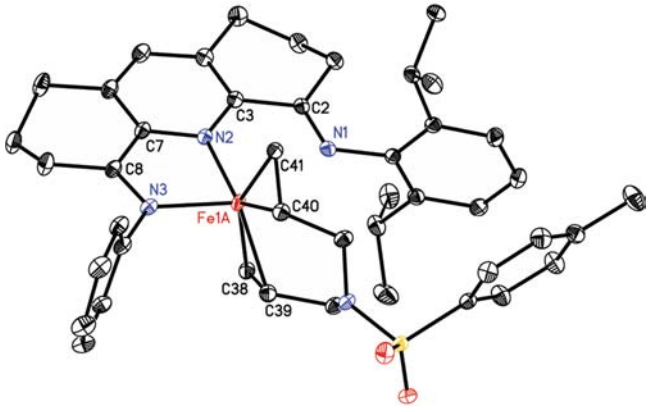

Figure 6. Solid-state structure for **3** at 30% ellipsoids. Hydrogen atoms and isopropyl substituents on one aryl ring omitted for clarity.

The electronic structure of **3** was further studied by solid-state ^{57}Fe Mössbauer spectroscopy and broken-symmetry DFT calculations. An isomer shift of 0.63 mm/s was measured at 80 K, a value significantly higher than those measured for the iron diyne and enyne metallacycles. Open shell DFT calculations converged to a BS(3,1) solution; this solution successfully reproduced the experimentally observed Mössbauer isomer shift and quadrupole splitting (Table 2). A qualitative molecular orbital diagram and spin density plot from the BS(3,1) solution is presented in Figure 7. The experimental and computational data are best described as a high-spin Fe(I) center (S_{Fe} = 3/2) antiferromagnetically coupled to a bis(imino)pyridine radical anion (S_{PDI} = 1/2). The difference in iron oxidation state, intermediate-spin Fe(III) versus high-spin Fe(I), accounts for the variance in observed isomer shift.

The catalytic competency of **3** was evaluated by allowing a benzene-d_6 solution of the compound to stand at 23 °C for several hours. Monitoring the reaction by ^{1}H NMR spectroscopy revealed little formation of the [3.2.0]azobicyloheptane; rather several new, paramagnetic iron compounds were observed. One of these was characterized by single crystal X-ray diffraction (see Supporting Information) and identified as the bis(imino)pyridine iron amide compound, ($^{iPr(TB)}$PDI)-FeN(Ts)(C_3H_5). This observed lack of reactivity with diallyl tosyl amine stands in contrast to the rapid cyclization of this substrate observed with (^{iPr}PDI)Fe(N_2)$_2$ which proceeded to complete conversion in less than 1 h.

The isolation of diene complex **3** raised the question whether iron olefin complexes or metallacycles are formed with more catalytically competent substrates. In the presence of 10 mol % of ($^{iPr(TB)}$PDI)Fe(N_2)$_2$ in benzene-d_6 solution, *N,N*-diallylaniline underwent quantitative cyclization and furnished the corresponding [3.2.0]azobicyloheptane in 3 h at 23 °C. Addition of 1 equiv of *N,N*-diallylaniline to a slurry of ($^{iPr(TB)}$PDI)Fe(N_2)$_2$ in hexane resulted in rapid precipitation of a purple powder identified as the iron metallacyclopentane, **4**, in 55% yield (eq 5).

As with the other metallacycles prepared in this work, **4** is paramagnetic with a solution magnetic moment of 2.9 μ_B

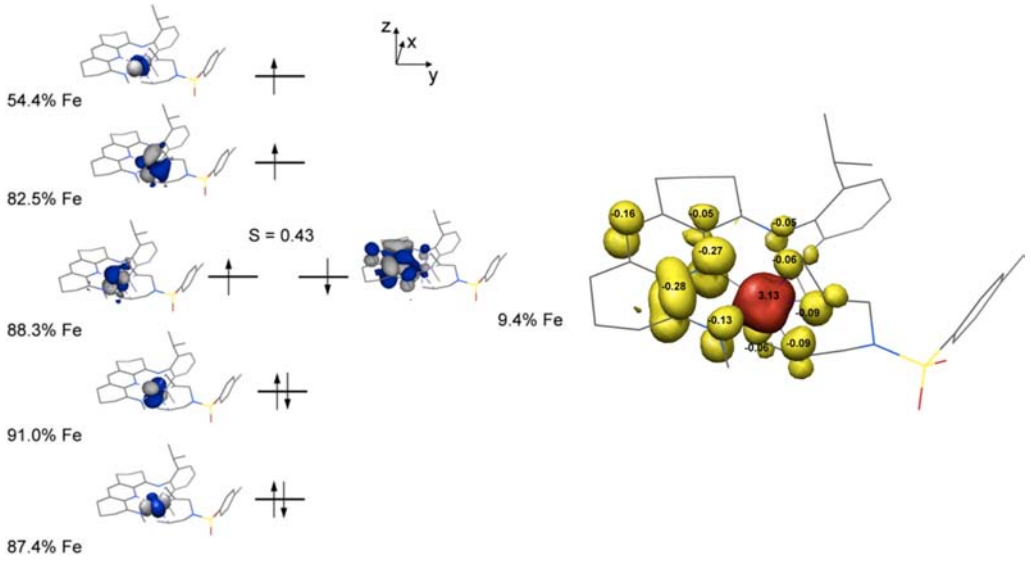

Figure 7. Qualitative molecular orbital diagram (left) and spin density plot (right) for the BS(3,1) solution for **3**.

dx.doi.org/10.1021/ja400895j | J. Am. Chem. Soc. 2013, 135, 4862−4877

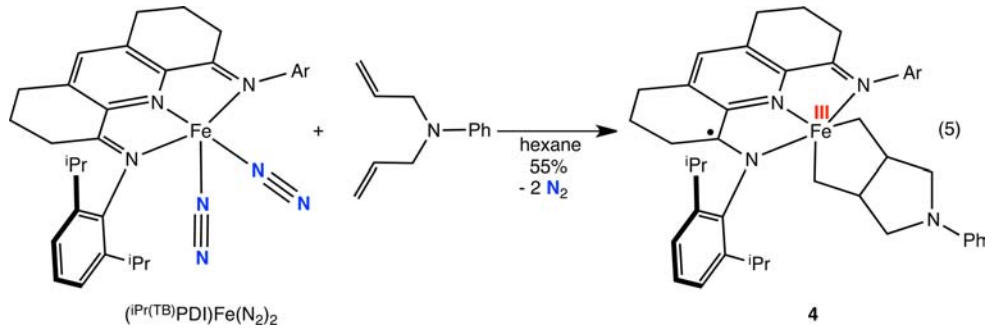

(benzene, 23 °C). The solid-state magnetic behavior was studied by SQUID magnetometry between 2 K and 300 K and established simple paramagnetic behavior (Figure S7). The benzene-d_6 NMR spectrum exhibited several broad peaks between −12 and 12 ppm. The zero-field ^{57}Fe Mössbauer spectrum exhibits an isomer shift of 0.30 mm/s and a quadrupole splitting of 2.66 mm/s. Within the series of the three metallacycles, the isomer shift steadily increases from **1** to **2** to **4** and is likely a result of the decreased s-character and hence reduced field strength when moving from two sp^2 to two sp^3 hydrocarbyl ligands.

The solid-state structure of **4** was determined by X-ray diffraction. The crystallographic data definitively establish formation of the bis(imino)pyridine iron metallacycle. The overall geometry of the metal center is best described as distorted square pyramidal with one of the carbon atoms of the metallacycle defining the apical position. The iron atom lies outside the plane of the chelate, and the carbon atoms that define the metallacycle are essentially perpendicular to the idealized iron-chelate plane. The C(39)−C(40) distance of 1.544(6) Å establishes carbon−carbon bond formation (Table 3).

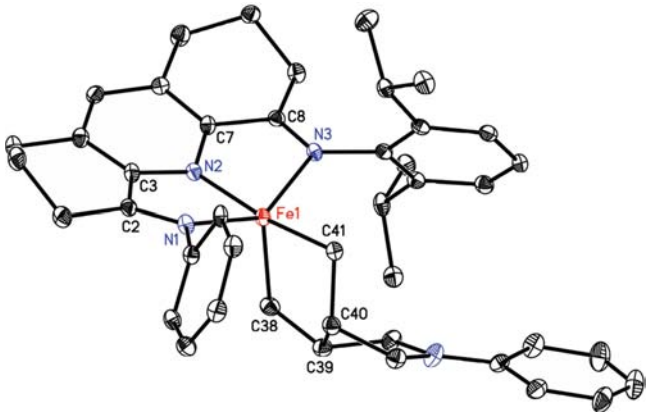

Figure 8. Solid-state structure for **4** at 30% ellipsoids. Isopropyl substituents on one aryl ring and hydrogen atoms omitted for clarity.

As with the other metallacycles and the diene compound, the electronic structure of **4** was examined with broken symmetry DFT calculations. The computed Mössbauer parameters are in good agreement with the experimental values and validate the accuracy of the optimized BS(3,1) solution. From this solution, a molecular orbital diagram and spin density plot were generated and are presented in Figure 9. As with the other metallacycles, the BS(3,1) solution corresponds to an intermediate-spin iron(III) compound with a bis(imino)-pyridine radical anion.

The discrepancy between isolation of iron diene complexes and metallacycles was explored with additional substrate modifications (Figure 10). Introduction of a 4-methoxysubstituent into *N*,*N*-diallylaniline and addition to ($^{iPr(TB)}$PDI)Fe$(N_2)_2$ furnished the iron metallacycle, **5** as determined by X-ray diffraction and Mössbauer spectroscopy. Because of the similarity between **4** and **5**, details for the latter compound are relegated to the Supporting Information.

An additional objective of these studies was to determine the influence of bis(imino)pyridine hapticity on the electronic structure of the iron diene compound. Because **3** exhibited a κ^2-bis(imino)pyridine ligand, an iron diene complex was targeted where coordination of all three nitrogens was retained. Addition of 1,5-hexadiene to a hexane slurry of ($^{iPr(TB)}$PDI)-Fe$(N_2)_2$ furnished a dark green solid identified as ($^{iPr(TB)}$PDI)-Fe(η^2, η^2-C_6H_{10}) (**6**) in 83% yield (Figure 10). A magnetic moment of 2.6 μB was measured in benzene-d_6 solution at 23 °C, diagnostic of an S = 1 ground state similar to other iron metallacycle and diene complexes isolated in this study. The Mössbauer isomer shift of 0.73 mm/s (Table 2) is also consistent with a high-spin iron compound and is slightly higher than the value of 0.63 mm/s observed with **3**.

The solid-state structure of **6** was determined by X-ray diffraction and a representation of the molecular structure is presented in Figure 11. Selected bond distances and angles are reported in the Supporting Information. The coordinated diene was disordered over two positions and successfully modeled. Only one orientation is shown in Figure 11. While the iron−imine bond distances are elongated (2.320(4) and 2.372(4) Å), the hapticity of the bis(imino)pyridine chelate is best described as κ^3. We note that all of the iron−ligand bonds are elongated, likely a consequence of the high spin state of the metal center. There is little perturbation to the C−C distances (1.39(1) and 1.36(1) Å) of the coordinated olefins, consistent with little backbonding from the high-spin iron center. The distortions to the bis(imino)pyridine (N_{imine}−C_{imine} = 1.300(6), 1.313(6) Å; C_{imine}−C_{ipso} = 1.442(7), 1.445(6) Å) chelate signal formation of one-electron-reduced radical anion. The combined magnetic, spectroscopic, and structural data are therefore consistent with a high-spin iron(I) center antiferromagnetically coupled to a bis(imino)pyridine radical anion. The electronic structure of **6** was also examined with broken symmetry DFT calculations. Similar to **3**, a BS(3,1) was obtained (Figure S15, Supporting Information). The only notable difference being that the spin density is more symmetrically distributed over the ligand likely arising from the more symmetric Fe−N_{imine} distances, a consequence of the κ^3 coordination of the chelate.

One final diene, diallylfluorene, was selected because it undergoes catalytic [2π + 2π] cyclization at 45 °C in the presence of either (^{iPr}PDI)Fe$(N_2)_2$ or ($^{iPr(TB)}$PDI)Fe$(N_2)_2$. The absence of a central nitrogen atom obviates potential

dx.doi.org/10.1021/ja400895j | J. Am. Chem. Soc. 2013, 135, 4862−4877

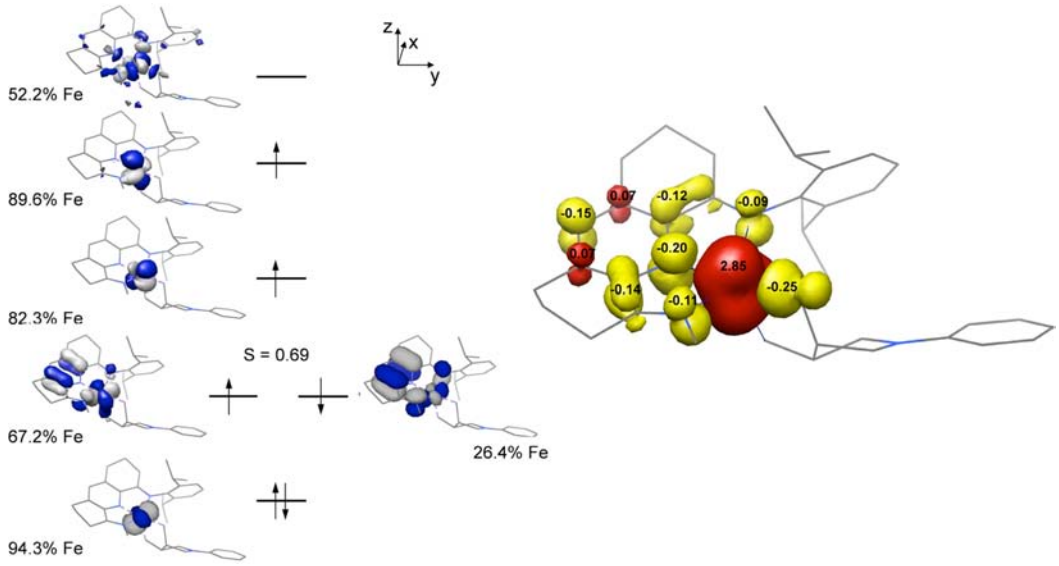

Figure 9. Qualitative molecular orbital diagram (left) and spin density plot (right) for the BS(3,1) solution for **4**.

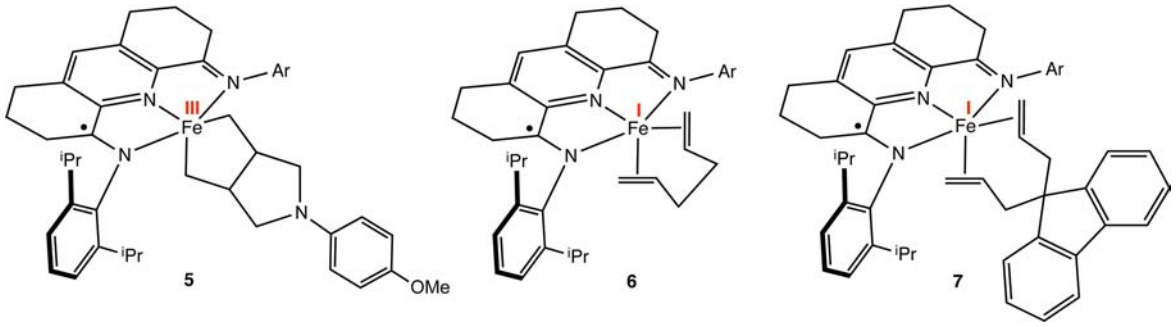

Figure 10. Additional bis(imino)pyridine iron metallacycle and diene complexes prepared in this study.

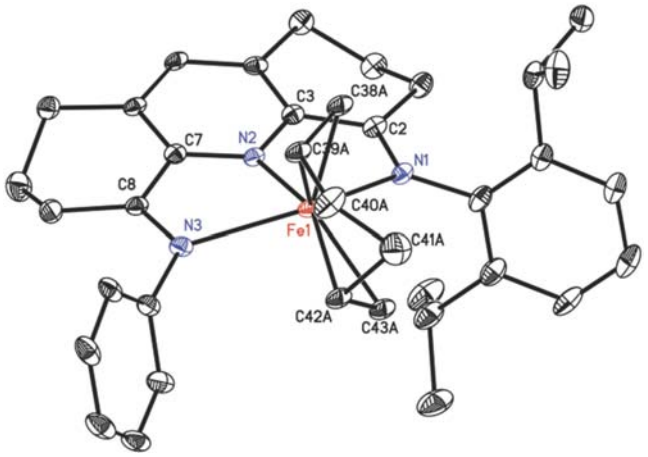

Figure 11. Solid-state structure for **6** at 30% probability ellipsoids. Isopropyl substituents on one aryl ring and hydrogen atoms omitted for clarity.

decomposition by iron amide formation. Addition of diallylfluorene to a hexane slurry of ($^{iPr(TB)}$PDI)Fe(N_2)$_2$ furnished dark green solid identified as the corresponding iron diene complex **7** in 45% yield (Figure 10). The benzene-d_6 solution magnetic moment of 2.9 μ_B recorded at 23 °C is consistent with an S = 1 compound. The Mössbauer isomer shift of 0.62 mm/s is comparable to the values of 0.63 and 0.73 mm/s reported for **3** and **6**, respectively, resulting in formulation as an iron diene complex rather than the metallacyclic alternative.

Comparison to Bis(imino)pyridine Iron Dialkyl Complexes. Our group has previously reported the synthesis of bis(imino)pyridine iron dialkyl complexes, (^{R}PDI)Fe(CH_2SiMe_3)$_2$,[65,66] each with an S = 2 ground state. Subsequent structural, spectroscopic, and computational studies established that these compounds are best described as *high-spin* Fe(III) derivatives antiferromagnetically coupled to a bis(imino)pyridine radical anion.[67] The high-spin ferric center in these compounds contrasts the intermediate-spin Fe(III) centers observed in metallacycles **1**, **2**, (^{iPr}PDI)Fe(diyne-**C**), (^{iPr}PDI)Fe(enyne-**D**), **4**, and **5**. What is the origin of this difference?

Because the bis(imino)pyridine chelates were different between the iron dialkyl and the metallacycles structurally characterized in this work, the synthesis of ($^{iPr(TB)}$PDI)Fe(CH_2SiMe_3)$_2$ was targeted. Dialkylation of ($^{iPr(TB)}$PDI)$FeCl_2$ with 2 equiv of $LiCH_2SiMe_3$[65] in diethyl ether followed by filtration and two recrystallizations from pentane at −35 °C furnished dark purple crystals in 24% yield identified as ($^{iPr(TB)}$PDI)Fe(CH_2SiMe_3)$_2$ (eq 6).

The zero-field ^{57}Fe Mössbauer spectrum of ($^{iPr(TB)}$PDI)Fe(CH_2SiMe_3)$_2$ was obtained at 80 K and established an isomer shift of 0.22 mm/s and a quadrupole splitting of 2.82 mm/s. These parameters are similar to those previously reported for (^{Et}PDI)Fe(CH_2SiMe_3)$_2$ (δ = 0.26 mm/s; ΔE_Q = 2.66 mm/s),

dx.doi.org/10.1021/ja400895j | J. Am. Chem. Soc. 2013, 135, 4862−4877

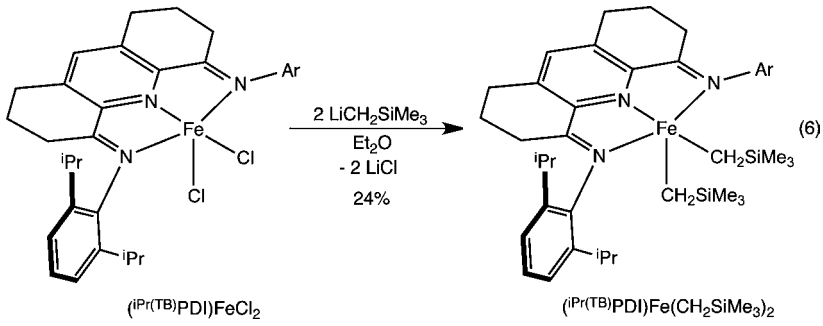

values ascribed to a high-spin ferric center antiferromagnetically coupled to a bis(imino)pyridine radical anion.[67] An unidentified second iron compound was detected in the Mössbauer spectrum (δ = 0.77 mm/s; ΔE_Q = 1.40 mm/s) that constituted up to 20% of the product mixture. A solution magnetic moment (Evans method) of 4.4 μ_B was measured in benzene at 23 °C, slightly lower than the value expected for four unpaired electrons and an S = 2 ground state. The low value reflects the presence of the second unidentified iron species.

The solid-state structure was determined by single crystal X-ray diffraction and a representation of the molecule is shown in Figure 12. Selected metrical parameters for the compound

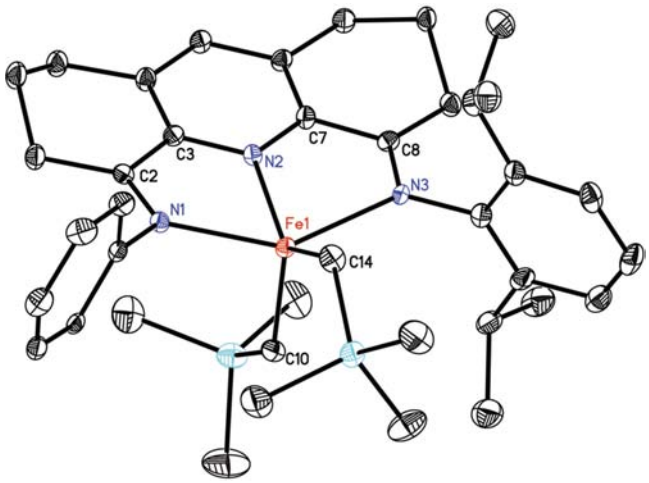

Figure 12. Solid-state structure of ($^{iPr(TB)}$PDI)Fe(CH_2SiMe_3)$_2$ at 30% probability ellipsoids. Isopropyl substituents on one aryl ring and hydrogen atoms omitted for clarity.

along with those previously reported for (^{iPr}PDI)Fe(CH_2SiMe_3)$_2$ are reported in Table 4. One notable structural feature is the transition of the overall molecular geometry to a more trigonal bipyramidal arrangement. In this view, the two alkyl ligands and the pyridine define the equatorial plane and the imine donors, albeit distorted due to the constraints of the chelate, occupy the axial positions. The angle between the two alkyl ligands, C(10)−Fe(1)−C(14), of 117.7(2)° is more open than the value of 84.8(2)° measured in the iron metallacycle, **4** which adopts a more square pyramidal geometry. The metrical parameters of the bis(imino)pyridine chelate in ($^{iPr(TB)}$PDI)Fe(CH_2SiMe_3)$_2$ are comparable to those previously reported for (^{iPr}PDI)Fe(CH_2SiMe_3)$_2$ and are consistent with one-electron reduction. In addition, the iron−nitrogen bonds from both imines (2.208(4) and 2.287(4) Å) and the central pyridine donor (2.012(3) Å) are elongated, consistent with a high-spin metal center.

Table 4. Selected Bond Distances (Å) and Angles (deg) for ($^{iPr(TB)}$PDI)Fe(CH_2SiMe_3)$_2$ and (^{iPr}PDI)Fe(CH_2SiMe_3)$_2$[65]

	($^{iPr(TB)}$PDI) Fe(CH_2SiMe_3)$_2$	(^{iPr}PDI) Fe(CH_2SiMe_3)$_2$
Fe(1)−N(1)	2.208(4)	2.203(2)
Fe(1)−N(2)	2.012(3)	2.013(2)
Fe(1)−N(3)	2.287(4)	2.263(3)
Fe(1)−C(10)	2.070(3)	2.062(3)
Fe(1)−C(14)	2.068(4)	2.054(3)
N(1)−C(2)	1.304(6)	1.302(3)
N(3)−C(8)	1.306(6)	1.301(3)
C(2)−C(3)	1.433(7)	1.448(3)
C(7)−C(8)	1.445(6)	1.454(3)
N(1)−Fe(1)−N(2)	74.7(1)	74.04(7)
N(1)−Fe(1)−N(3)	144.8(1)	141.07(7)
N(2)−Fe(1)−N(3)	73.2(1)	72.88(7)
C(10)−Fe(1)−C(14)	117.6(2)	112.0(1)
C(10)−Fe(1)−N(1)	101.5(1)	103.37(9)
C(10)−Fe(1)−N(2)	107.2(1)	107.93(9)
C(10)−Fe(1)−N(3)	101.5(1)	105.86(9)
C(14)−Fe(1)−N(1)	98.6(1)	98.2(1)
C(14)−Fe(1)−N(2)	135.1(1)	140.0(1)
C(14)−Fe(1)−N(3)	93.8(1)	94.1(1)

The electronic structure of ($^{iPr(TB)}$PDI)Fe(CH_2SiMe_3)$_2$ was also examined by full molecule DFT calculations. A BS(5,1) solution, corresponding to a high-spin iron(III) center antiferromagnetically coupled to a bis(imino)pyridine radical anion, successfully reproduced both the metrical and Mössbauer parameters. A qualitative molecular orbital diagram and spin density plot from this solution are reported in the Supporting Information (Figure S16). The combined structural, spectroscopic, and computational data on ($^{iPr(TB)}$PDI)Fe(CH_2SiMe_3)$_2$ are most consistent with an overall S = 2 complex derived from a high-spin ferric center antiferromagnetically coupled to a bis(imino)pyridine radical anion. This electronic structure is analogous to all other (^{R}PDI)Fe(CH_2SiMe_3)$_2$ compounds prepared to date, suggesting that the identity of the specific bis(imino)pyridine has little influence on the overall electronic structure of the compound.

What then is the origin of the difference in spin state between the iron metallacycles (intermediate-spin ferric) and the dialkyl complexes (high-spin ferric)? To probe this issue, DFT calculations were performed on the hypothetical bis(imino)pyridine iron dimethyl complex, ($^{iPr(TB)}$PDI)Fe(CH_3)$_2$. Square pyramidal and trigonal bipyramidal geometries were considered using the iron metallacycle, **4**, and the iron dialkyl, ($^{iPr(TB)}$PDI)Fe(CH_2SiMe_3)$_2$, metrical parameters as initiating points. For each geometry, BS(5,1) and BS(3,1) possibilities were evaluated, corresponding to high and intermediate-spin

dx.doi.org/10.1021/ja400895j | J. Am. Chem. Soc. 2013, 135, 4862−4877

Scheme 3. Proposed Catalytic Cycle for the Hydrogenative Cyclization of Enynes (illustrated) and Diynes (implied) with Redox-Active Bis(imino)pyridine Iron Complexes

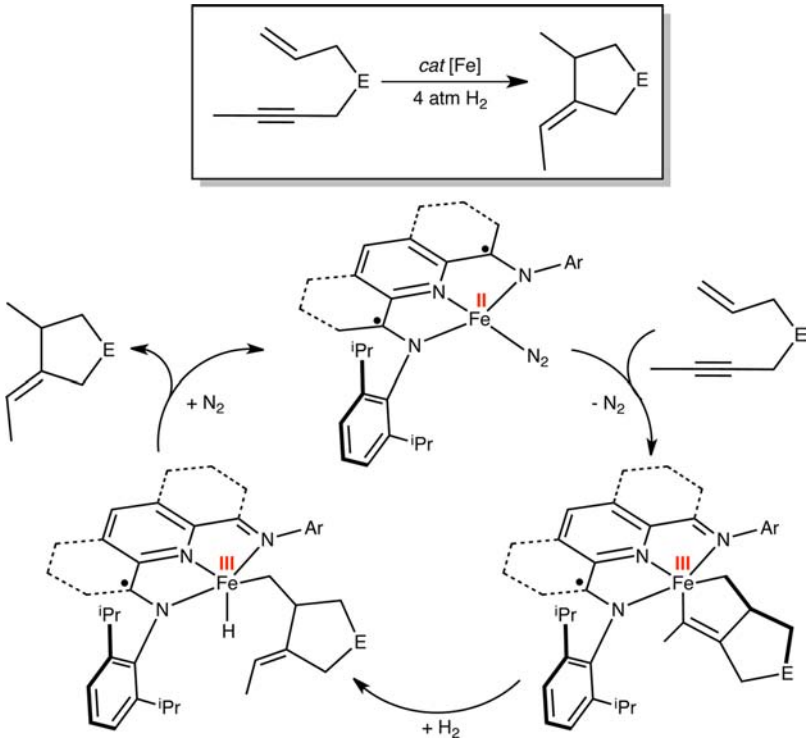

Scheme 4. Proposed Catalytic Cycle for the $[2\pi + 2\pi]$ Cyclization of α,ω-Dienes with Redox-Active Bis(imino)pyridine Iron Complexes

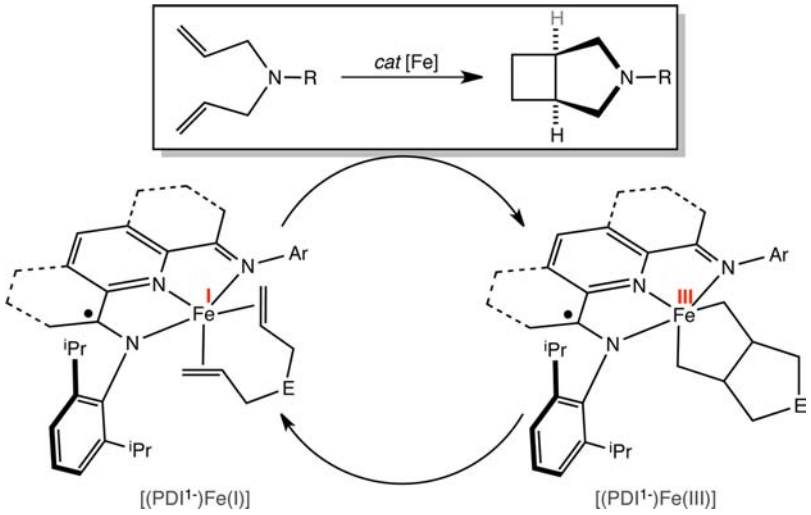

ferric centers, respectively. For both spin states, the square pyramidal geometry was energetically favored considerably (see Table S8 in Supporting Information for details) over the trigonal bipyramidal alternative. Between the BS(3,1) and BS(5,1) solutions in the square pyramidal regime, the S = 1, BS(3,1) possibility was favored by ∼13 kcal/mol. This result is anticipated as the BS(3,1) solution corresponds to the preferred electronic structure description of the input molecule. Following optimization from the square pyramidal metrical parameters, both spin states converged, producing C−Fe−C angles of 93.9° (BS(3,1)) and 92.2° (BS(5,1)), close to the value observed experimentally in **4**. In the case of the S = 1, BS(3,1) input, optimization from the trigonal bipyramidal metrical parameters converged to a solution closer to those expected for a square pyramid (C−Fe−C angle of 91.3°). On the basis of these findings, we conclude that the BS(3,1) solution and hence S = 1 ground state in a square pyramidal geometry is the preferred electronic and steric arrangement for bis(imino)pyridine iron dialkyl and metallacycles. The exceptions are the $(^{R}PDI)Fe(CH_2SiMe_3)_2$ compounds which are S = 2. The steric pressure resulting from the large alkyl groups favor a more idealized trigonal bipyramidal geometry with elongated Fe−C bonds and hence an overall weaker ligand field. Unfortunately, we[66] and others[68] have failed to synthesize other bis(imino)pyridine iron dialkyl complex with different hydrocarbyl substituents.

dx.doi.org/10.1021/ja400895j | J. Am. Chem. Soc. 2013, 135, 4862−4877

Electronic Structure Summary and Implications for Catalytic Turnover. The isolation, structural characterization, and elucidation of the electronic structure of bis(imino)pyridine iron diene and various metallacycle complexes provides new insight into the mechanism of turnover and the flow of electrons during the critical bond-forming events that comprise the catalytic cycles. A mechanism accounting for the electronic structures of the iron metallacycles formed during hydrogenative enyne cyclization is presented in Scheme 3. The pathway for diyne cyclization would be analogous and is not explicitly illustrated. Recent studies on the electronic structure of the parent iron precatalyst, (^{iPr}PDI)FeN$_2$, established an intermediate-spin iron(II) compound (S_{Fe} = 1) with a triplet diradical bis(imino)pyridine dianion.[51] Substitution of the dinitrogen ligand by the substrate results in metallacycle formation, including construction of the C−C bond. The enyne cyclization event forms an S = 1 iron compound with formal one-electron oxidation events occurring both at the bis(imino)pyridine (e.g., $[PDI]^{2-} \rightarrow [PDI]^{1-}$) and iron (e.g., $Fe^{2+} \rightarrow Fe^{3+}$). Turnover-limiting hydrogenation[36] forms the bis(imino)pyridine iron alkyl (or alkenyl) hydride, which by analogy to iron dialkyls[67] is likely an iron(III) compound with a one-electron reduced chelate. Because the S = 2 ground state of the iron dialkyls is anomalous and results from the steric pressure imparted by large hydrocarbyl ligands, it is likely that the bis(imino)pyridine iron alkyl hydride intermediate has an S = 1 ground state. Thus, at high concentrations of substrate where the formation of the iron dinitrogen complex is minimized, the catalytic cycle involves ferric intermediates with a bis(imino)pyridine radical anion where an S = 1 spin state is maintained.

A proposed mechanism for the thermal bis(imino)pyridine iron-catalyzed [2π + 2π] cycloaddition of α,ω-dienes is presented in Scheme 4. In this case, both iron diene and metallacycle complexes were isolated and fully characterized, providing more complete insight into the electronic structure of iron compounds formed along the catalytic reaction coordinate. Iron diene complexes with both κ^2 and κ^3 bis(imino)pyridine ligands were synthesized and show no variance in electronic structure, demonstrating that if imine dissociation is indeed operative, it does not change the physical oxidation state of the iron or the bis(imino)pyridine chelate. Unlike our initial proposal suggesting that ferrous oxidation state was maintained throughout the catalytic cycle,[40] the electronic structure data presented in this report clearly support an Fe(I)−Fe(III) couple for catalytic [2π + 2π] cycloaddition. We note that a similar redox couple has also been invoked in iron-catalyzed cross-coupling reactions.[69,70] The oxidative event that promotes iron metallacycle and hence C−C bond formation is metal based, as the high-spin Fe(I) diene complex converts to intermediate-spin Fe(III). Notably, the oxidation state of the chelate is maintained as the bis(imino)pyridine remains in the radical anion form through the catalytic cycle.

The most intriguing step of the catalytic cycle shown in Scheme 4 is the sp^3−sp^3 reductive elimination reaction. It is the facility of this step that enables cyclobutane formation and gives rise to the unique catalytic activity observed with the bis(imino)pyridine iron catalysts. Previous studies have focused on the mechanism of stoichiometric sp^3−sp^3 C−C reductive elimination from first row transition metals and provide a foundation for the bis(imino)pyridine iron compounds described here.[71] Grubbs and co-workers[72] reported C−C reductive elimination from low spin, Ni(II) phosphine nickelocyclopentanes and found that stoichiometric cyclobutane formation was favored when the nickel metallacycle was four coordinate. Phosphine dissociation to form three-coordinate derivatives opened a coordinate site for sequential β-hydrogen and C−H reductive eliminations resulting in formation of linear butenes. At higher phosphine concentrations, five-coordinate Ni(II) complexes persisted and resulted in exclusive formation of ethylene arising from cycloreversion of the metallacycle. More recently, Xu and Bernskoetter[73] have investigated ethane formation from the low-spin, six-coordinate Co(III) dimethyl complex, *cis,mer*-$(Me_3P)_3CoMe_2I$, in chemistry related to that initially described by Yamamoto.[74] A combination of kinetic studies and crossover and isotopic labeling experiments coupled with solvent effects and phosphine inhibition studies all supported a concerted C−C bond-forming event from an unobserved five-coordinate Co(III) intermediate, similar to established C−C reductive elimination pathways in Pt(IV) chemistry. In the cobalt case, however, the generation of an S = 1 four-coordinate cobalt product necessitates a spin-state change along the reaction coordinate.

More germane to this study is Kochi and co-workers'[75] seminal report of the relative rates and favored pathways of sp^3−sp^3 C−C reductive elimination as a function of iron oxidation state. Variants of Yamamoto's $(bipy)_2FeR_2$ (R = Me, Et, ^{n}Pr, ^{n}Bu, cyclo-$(CH_2)_4$) complexes,[76] where the alkyl groups are in a cis configuration, formed the basis for this study. For the neutral, formally ferrous compound, $(bipy)_2FeEt_2$, ethylene and ethane were the principal organic products, consistent with a pathway involving κ^2−κ^1 interconversion of the bipy ligand, opening a coordination site for β-hydrogen elimination. Reductive elimination of a C−H bond accounts for the observed CH_3−CH_3 product. Electrochemical or chemical oxidation of the $(bipy)_2FeR_2$ compounds furnished low-spin Fe(III) derivatives that decomposed principally by iron−carbon bond homolysis. For the ferracyclopentane example, $(bipy)_2Fe$-(cyclo-$(CH_2)_4$, cyclobutane was the dominant product of the radical pathway. Continued oxidation to the Fe(IV) dications, $[(bipy)_2FeR_2]^{2+}$, by electrochemical methods cleanly generated coupled alkyl products from exclusive sp^3−sp^3 C−C reductive elimination. While mechanistic studies were limited by the transient nature of the iron dications, a concerted pathway was favored. Kochi also noted that the relative rates of decomposition markedly increased as a function of formal iron oxidation state, where Fe(II) < Fe(III) < Fe(IV).

The isolation and elucidation of the electronic structures of **4** and **5** provides important insight into the catalytic competency of the sp^3−sp^3 C−C reductive elimination and the role and importance of the redox-active bis(imino)pyridine ligand. On the basis of the work of Kochi, it is likely that if the bis(imino)pyridine iron metallacycles maintained their formal Fe(II) oxidation state where the chelate was in a *redox-innocent*, neutral form, cyclobutane formation would be inhibited. Because the iron complexes are five coordinate and have open coordination sites, it is also likely with a lower metal oxidation state, β-hydrogen elimination would become competitive with C−C reductive elimination and the products of the reaction would likely be altered. The redox-active bis(imino)pyridine is therefore an important contributor to catalytic activity, as it enables formation of an intermediate-spin ferric complex which facilitates C−C reductive elimination. It is also plausible that this pathway proceeds by iron−carbon bond homolysis, and additional experimentation is required to

dx.doi.org/10.1021/ja400895j | J. Am. Chem. Soc. 2013, 135, 4862−4877

evaluate such a possibility. We note that in our initial communication,[40] deuterium-labeling experiments were reported that supported retention of stereochemistry during catalytic [2π + 2π] cycloaddition, suggesting that if Fe−C homolysis is indeed operative, ring closure and cyclobutane formation is faster than C−C bond rotation.

All of the experimental data support an $S = 1$ spin surface for iron-catalyzed [2π + 2π] cycloaddition. If the catalytic reaction is completed in the presence of excess dinitrogen, $S = 0$ bis(imino)pyridine iron dinitrogen complexes can be isolated that maintain their catalytic performance, suggesting that the iron complexes can pass from $S = 0$ to $S = 1$ reaction surfaces with impunity. During turnover, once product has been released, the bis(imino)pyridine maintains the radical anion oxidation state and diene coordination occurs at a high-spin Fe(I) center. This oxidation state is likely beneficial as Fe(0) complexes may be subject to decomposition by chelate dissociation and formation of metallic iron. Such a pathway inhibits catalytic turnover in the Grubbs nickel compounds.[72] Thus, the redox-active chelates serve multiple purposes that enable the unique catalytic [2π + 2π] cycloaddition observed with bis(imino)pyridine iron compounds. By maintaining their radical anion form, these versatile ligands inhibit decomposition by deposition of metallic iron as well as enable iron(III) metallacycles that favor sp^3−sp^3 C−C reductive elimination over other competing processes such as β-hydrogen elimination. These insights should prove useful for future catalyst and reaction development.

CONCLUDING REMARKS

A family of bis(imino)pyridine iron metallacycles has been synthesized, isolated, and structurally characterized, allowing elucidation of the electronic structure of important intermediates in iron-catalyzed hydrogenative cyclization and cycloaddition reactions. All of the experimental and computational data support a monoreduced bis(imino)pyridine radical anion throughout catalytic turnover and that an Fe(I)−Fe(III) cycle is operative for C−C bond formation. These features enable a sufficiently high oxidation state iron complex to enable facile sp^3−sp^3 C−C reductive elimination and avoid reduced iron compounds that would result in catalyst decomposition by metal deposition.

EXPERIMENTAL SECTION[77]

Preparation of ($^{iPr(TB)}$PDI)Fe(N_2)$_2$. A 100 mL round-bottom flask was charged with 0.070 g (3.03 mmol) of sodium metal and approximately 50 mL of toluene. With stirring, 14.0 g (69.3 mmol) of mercury was added to the flask followed by 0.400 g (0.606 mmol) of ($^{iPr(TB)}$PDI)FeCl_2. The reaction mixture was stirred for 14 h after which time the resulting dark green solution was filtered through Celite, and the toluene was removed in vacuo. The resulting green/brown solid was recrystallized from pentane at −35 °C to yield 0.240 g (61%) of ($^{iPr(TB)}$PDI)Fe(N_2)$_2$ as a dark green solid. ^{1}H NMR (benzene-d_6, 20 °C): δ = 0.64 (bs, 8H, N=CCH_2CH_2CH_2), 0.85 (d, 12H, CH(CH_3)$_2$), 1.73 (bs, 4H, N=CCH_2), 2.68 (bs, 4H, CH(CH$_3$)$_2$), 7.36−7.46 (m, 6H, *m* and *p*-Ar), *p*-pyr and CH(CH_3)$_2$ not located. Anal. for $C_{37}H_{47}N_7Fe$: Calcd C, 68.83; H, 7.34; N, 15.19. Found: C, 68.95; H, 7.16; N, 14.79. IR (pentane): ν (N_2) = 2124 and 2061 cm^{-1} (five coordinate); 2025 cm^{-1} (four coordinate).

Preparation of ($^{iPr(TB)}$PDI)Fe(*N*,*N*-Dibut-2-ynyl-4-methylbenzenesulfonamide) (1). A 20 mL scintillation vial was charged with 0.050 g (0.077 mmol) of ($^{iPr(TB)}$PDI)Fe(N_2)$_2$ and approximately 2 mL of hexanes. The slurry was stirred for 5 min before 0.022 g (0.081 mmol) of *N*,*N*-dibut-2-ynyl-4-methylbenzenesulfonamide in approximately 2 mL of hexanes was added. The resulting reaction mixture was stirred for 5 min and then filtered. A red solid was collected and was washed with hexanes (2 × 1 mL), yielding 0.056 g (84%) of the desired product as a dark red solid. Anal. for $C_{52}H_{64}N_4O_2SFe$: Calcd C, 72.20; H, 7.46; N, 6.48. Found: C, 71.96; H, 7.27; N, 6.22. Magnetic susceptibility (Evans): μ_{eff} = 2.8 μ_B (benzene-d_6, 23 °C).

Preparation of ($^{iPr(TB)}$PDI)Fe(*N*-Allyl-*N*-(but-2-ynyl)-4-methylbenzenesulfonamide) (2). This compound was prepared in a fashion similar to that for ($^{iPr(TB)}$PDI)Fe(*N*,*N*-dibut-2-ynyl-4-methylbenzenesulfonamide) using 0.050 g (0.077 mmol) of ($^{iPr(TB)}$PDI)Fe(N_2)$_2$ and 0.021 g (0.081 mmol) of *N*-allyl-*N*-(but-2-ynyl)-4-methylbenzenesulfonamide in approximately 2 mL of hexanes. This procedure yielded 0.045 g (68%) of the desired iron metallacycle as a dark red solid. ^{1}H NMR (benzene-d_6, 20 °C): δ = −102.07, −18.29, −16.79, −3.17, −0.02, 0.18, 2.38, 3.43, 4.08, 4.48, 6.58, 7.43, 9.52, 9.91, 10.20, 13.48, 13.98, 20.74, 26.94, 29.55, 30.18, 33.58, 36.55, 51.06, 53.69, 127.48, 241.11 ppm. Anal. for $C_{51}H_{64}N_4O_2SFe$: Calcd C, 71.81; H, 7.56; N, 6.57. Found: C, 71.71; H, 7.29; N, 6.33. Magnetic susceptibility (Evans): μ_{eff} = 2.8 μ_B (benzene-d_6, 23 °C).

Preparation of ($^{iPr(TB)}$PDI)Fe(*N*,*N*-diallylaniline) (4). This compound was prepared in a similar fashion to ($^{iPr(TB)}$PDI)Fe(*N*,*N*-dibut-2-ynyl-4-methylbenzenesulfonamide) using 0.075 g (0.116 mmol) of ($^{iPr(TB)}$PDI)Fe(N_2)$_2$ and 0.060 g (0.348 mmol) of *N*,*N*-diallylaniline in approximately 2 mL of hexanes. This procedure yielded 0.048 g (55% yield) of a dark purple solid identified as the desired iron metallacycle. ^{1}H NMR (benzene-d_6, 20 °C): δ = −10.41, −5.03, −1.16, 2.50, 3.67, 5.22, 8.62, 9.27 ppm. Anal. for $C_{49}H_{62}N_4Fe$: Calcd C, 77.14; H, 8.19; N, 7.34. Found: C, 76.85; H, 8.23; N, 6.97. Magnetic susceptibility (Evans): μ_{eff} = 2.9 μ_B (benzene-d_6, 23 °C).

Preparation of ($^{iPr(TB)}$PDI)Fe(CH_2SiMe_3)$_2$. A 20 mL scintillation vial was charged with 0.450 g (0.454 mmol) of ($^{iPr(TB)}$PDI)$FeCl_2$ and approximately 10 mL of diethyl ether, and the resulting slurry was frozen in a liquid nitrogen-cooled cold well. A second 20 mL scintillation vial was charged with 0.088 g (0.930 mmol) of $LiCH_2SiMe_3$ and approximately 2 mL of diethyl ether. This solution was added dropwise to the frozen contents of the first vial. The reaction mixture was then stirred at room temperature for 6 h, slowly forming a dark purple solution. The solvent was then removed in vacuo, reconstituted in approximately 10 mL of toluene, and filtered through Celite. The solvent was again removed in vacuo, and the resulting purple solid was twice recrystallized from small portions of diethyl ether, yielding 0.174 g (24% yield) of a dark purple solid identified as predominately ($^{iPr(TB)}$PDI)Fe(CH_2SiMe_3)$_2$ by Mössbauer spectroscopy.

ASSOCIATED CONTENT

Supporting Information

Additional experimental procedures, including general considerations and spectroscopic and computational details. Representative zero-field ^{57}Fe Mössbauer spectra and crystallographic data in cif format for **1**, **2**, **3**, **4**, ($^{iPr(TB)}$PDI)FeN(Ts)(Allyl), **6**, and ($^{iPr(TB)}$PDI)Fe(CH_2SiMe_3)$_2$. This material is available free of charge via the Internet at http://pubs.acs.org.

AUTHOR INFORMATION

Corresponding Author

pchirik@princeton.edu

Notes

The authors declare no competing financial interest.

ACKNOWLEDGMENTS

We thank the U.S. National Science Foundation and Deutsche Forschungsgemeinschaft for a Cooperative Activities in Chemistry between U.S. and German Investigators grant (CHE-1026084). We also thank Dr. Daigoro Hirai and Prof. Robert Cava for assistance with the SQUID measurements. S.P.S. thanks the Natural Sciences and Engineering Research Council of Canada for a predoctoral fellowship.

REFERENCES

(1) (a) Lautens, M.; Klute, W.; Tam, W. *Chem. Rev.* **1996**, *96*, 49. (b) Ojima, I.; Tzamarioudaki, M.; Li, Z.; Donovan, R. J. *Chem. Rev.* **1996**, *96*, 635.
(2) Aubert, C.; Buisine, O.; Malacria, M. *Chem. Rev.* **2002**, *102*, 813.
(3) Zhang, Z.; Zhu, G.; Tong, X.; Wang, F.; Xie, X.; Wang, J.; Jiang, L. *Curr. Org. Chem.* **2006**, *10*, 1457.
(4) Watson, I. D. G.; Toste, F. D. *Chem. Sci.* **2012**, *3*, 2899.
(5) Yamamoto, Y. *Chem. Rev.* **2012**, *112*, 4736.
(6) Inglesby, P. A.; Evans, P. A. *Chem. Soc. Rev.* **2010**, *39*, 2791.
(7) Aubert, C.; Malacria, M.; Ollivier, C. *Sci. Synth.* **2011**, *3*, 145.
(8) Schore, N. E. In *Comprehensive Organic Synthesis*; Trost, B. M., Fleming, I., Eds.; Pergamon: Oxford, 1991; Vol *5*.
(9) Vollhardt, K. P. C. *Angew. Chem., Int. Ed. Engl.* **1984**, *23*, 536.
(10) Chopade, P. R.; Louie, J. *Adv. Synth. Catal.* **2006**, *348*, 2307.
(11) Murakami, M.; Itami, K.; Ito, Y. *J. Am. Chem. Soc.* **1996**, *118*, 11672.
(12) Gutnov, A.; Heller, B.; Fischer, C.; Drexler, H.-J.; Spannenberg, A.; Sundermann, B.; Sundermann, C. *Angew. Chem., Int. Ed.* **2004**, *43*, 3795.
(13) Amin, J.; Richards, C. J. **2012**, *48*, 10192.
(14) Trost, B. M.; Romero, D. L.; Rise, F. *J. Am. Chem. Soc.* **1994**, *116*, 4268.
(15) Negishi, E.; Takahashi, T. *Acc. Chem. Res.* **1994**, *27*, 124.
(16) Sigman, M. S.; Kerr, C. E.; Eaton, B. E. *J. Am. Chem. Soc.* **1993**, *115*, 7545.
(17) Masutomi, K.; Sakiyama, N.; Noguchi, K.; Tanaka, K. *Angew. Chem., Int. Ed.* **2012**, *51*, 13031.
(18) Grigg, R.; Malone, J. F.; Mitchell, T. R. B.; Ramasubbu, A.; Scott, R. M. *J. Chem. Soc., Perkin Trans. 1* **1984**, 1745.
(19) (a) Kisanga, P.; Goj, L. A.; Widenhofer, R. A. *J. Org. Chem.* **2001**, *66*, 635. (b) Goj, L. A.; Widenhofer, R. A. *J. Am. Chem. Soc.* **2001**, *123*, 11133. (C) Goj, L. A.; Cisneros, G. A.; Yang, W.; Windenhofer, R. A. *J. Organomet. Chem.* **2004**, *689*, 2845.
(20) (a) Bray, K. L.; Charmant, J. P. H.; Fairlamb, I. J. S.; Lloyd-Jones, G. C. *Chem.—Eur. J.* **2001**, *7*, 4205. (b) Bray, K. L.; Lloyd-Jones, G. C. *Eur. J. Org. Chem.* **2001**, 1635.
(21) Ritter, S. K. *Chem. Eng. News*, June 25, **2012**, 12−18.
(22) Junge, K.; Schröder, K.; Beller, M. *Chem. Commun.* **2011**, *47*, 4849.
(23) Gaillard, S.; Renaud, J.-L. *ChemSusChem* **2008**, *1*, 505.
(24) Plietker, B. *Iron Catalysis in Organic Chemistry: Reactions and Applications*; Wiley-VCH: Weinheim, 2008.
(25) Bauer, E. B. *Curr. Org. Chem.* **2008**, *12*, 1341.
(26) Takacs, J. M.; Anderson, L. G.; Bindu Madhavan, G. V.; Creswell, M. W.; Seely, F. L.; Devroy, W. F. *Organometallics* **1986**, *5*, 2395.
(27) Takacs, J. M.; Weidner, J. J.; Newsome, P. W.; Takacs, B. E.; Chidambaram, R.; Shoemaker, R. *J. Org. Chem.* **1995**, *60*, 3473.
(28) Takacs, J. M.; Boito, S. C. *Tetrahedron Lett.* **1995**, *36*, 2941.
(29) Nieto-Oberhuber, C.; Muñoz, M. P.; Lopez, S.; Jimenez-Nunez, E.; Nevado, C.; Herrero-Gomez, E.; Raducan, M.; Echavarren, A. M. *Chem.—Eur. J.* **2006**, *12*, 1677.
(30) Hata, T.; Sujaku, S.; Hirone, N.; Nakano, K.; Imoto, J.; Imade, H.; Urabe, H. *Chem.—Eur. J.* **2011**, *17*, 14593.
(31) Fürstner, A.; Majima, K.; Martin, R.; Krause, H.; Kattnig, E.; Goddard, R.; Lehmann, C. W. *J. Am. Chem. Soc.* **2008**, *41*, 1500.
(32) Bart, S. C.; Lobkovsky, E.; Chirik, P. J. *J. Am. Chem. Soc.* **2004**, *126*, 13794.
(33) Russell, S. K.; Darmon, J. M.; Lobkovsky, E.; Chirik, P. J. *Inorg. Chem.* **2010**, *49*, 2782.
(34) (a) Archer, A. M.; Bouwkamp, M. W.; Cortez, M.-P.; Lobkovsky, E.; Chirik, P. J. *Organometallics* **2006**, *25*, 4269. (b) Trovitch, R. J.; Lobkovsky, E.; Bill, E.; Chirik, P. J. *Organometallics* **2008**, *27*, 1470. (c) Yu, R. P.; Darmon, J. M.; Hoyt, J. M.; Margulieux, G. W.; Turner, Z. R.; Chirik, P. J. *ACS Catal.* **2012**, *2*, 1760.
(35) (a) Tondreau, A. M.; Atienza, C. C. H.; Weller, K. J.; Nye, S. A.; Lewis, K. M.; Delis, J. G. P.; Chirik, P. J. *Science* **2012**, *335*, 567. (b) Atienza, C. C. H.; Tondreau, A. M.; Weller, K. J.; Lewis, K. M.; Cruse, R. W.; Nye, S. A.; Boyer, J. L.; Delis, J. G. P.; Chirik, P. J. *ACS Catal.* **2012**, *2*, 2169.
(36) Sylvester, K. T.; Chirik, P. J. *J. Am. Chem. Soc.* **2009**, *131*, 8772.
(37) Jang, H.-Y.; Krische, M. J. *Acc. Chem. Res.* **2004**, *37*, 653.
(38) Jang, H.-Y.; Krische, M. J. *J. Am. Chem. Soc.* **2004**, *126*, 7875.
(39) Jang, H.-Y.; Hughes, D. W.; Gong, H.; Zhang, J.; Brodbelt, J. S.; Krische, M. J. *J. Am. Chem. Soc.* **2005**, *127*, 6174.
(40) Bouwkamp, M. W.; Bowman, A. C.; Lobkovsky, E.; Chirik, P. J. *J. Am. Chem. Soc.* **2006**, *128*, 13340.
(41) Russell, S. K.; Lobkovsky, E.; Chirik, P. J. *J. Am. Chem. Soc.* **2011**, *133*, 8858.
(42) (a) Jiang, X.; Chen, X.; Ma, S. *Angew. Chem., Int. Ed.* **2006**, *118*, 8177. (b) Ohno, H.; Mizutani, T.; Kadoh, Y.; Miyamura, K.; Tanaka, T. *Angew. Chem., Int. Ed.* **2005**, *44*, 5113. (c) Shen, Q.; Hammond, G. B. *J. Am. Chem. Soc.* **2002**, *124*, 6534. (d) Brummond, K. M.; Chen, D. *Org. Lett.* **2005**, *7*, 3473. (e) Oh, C. H.; Gupta, A. K.; Park, D. I.; Kim, N. *Chem. Commun.* **2005**, 5670. (f) Nicholas, K. M. *J. Am. Chem. Soc.* **1975**, *97*, 3255. (g) Neoh, S. B.; Garratt, P. J. *J. Org. Chem.* **1979**, *44*, 2667. (h) Toda, F.; Tdnaka, K.; Sano, I.; Isozaki, T. *Angew. Chem., Int. Ed.* **1994**, *33*, 1757. (i) Saito, S.; Hirayama, K.; Kabuto, C.; Yamamoto, Y. *J. Am. Chem. Soc.* **2000**, *122*, 10776. (j) Alcaide, B.; Almendros, P.; Aragoncillo, C. *Chem. Soc. Rev.* **2010**, *39*, 783.
(43) de Bruin, B.; Bill, E.; Bothe, E.; Weyhermüller, T.; Wieghardt, K. *Inorg. Chem.* **2000**, *39*, 2936.
(44) Chirik, P. J. *Inorg. Chem.* **2011**, *50*, 9737.
(45) Knijnenburg, Q.; Gambarotta, S.; Budzelaar, P. H. M. *Dalton Trans.* **2006**, 5442.
(46) Bart, S. C.; Chlopek, K.; Bill, E.; Bouwkamp, M. W.; Lobkovsky, E.; Neese, F.; Wieghardt, K.; Chirik, P. J. *J. Am. Chem. Soc.* **2006**, *128*, 13901.
(47) Chirik, P. J.; Wieghardt, K. *Science* **2010**, *327*, 794.
(48) Campora, J.; Palma, P.; Carmona, E. *Coord. Chem. Rev.* **1999**, *193−195*, 207.
(49) Crumpton-Bregel, D. M.; Goldberg, K. I. *J. Am. Chem. Soc.* **2003**, *125*, 9442.
(50) Appukuttan, V. K.; Liu, Y.; Son, B. C.; Ha, C.; Suh, H.; Kim, I. *Organometallics* **2011**, *30*, 2285.
(51) Stieber, S. C. E.; Milsmann, C.; Hoyt, J. M.; Turner, Z. R.; Finkelstein, K. D.; Wieghardt, K.; DeBeer, S.; Chirik, P. J. *Inorg. Chem.* **2012**, *51*, 3770.
(52) Knijnenburg, Q.; Gambarotta, S.; Budzelaar, P. H. M. *Dalton Trans.* **2006**, 5442.
(53) Bart, S. C.; Lobkovsky, E.; Bill, E.; Wieghardt, K.; Chirik, P. J. *Inorg. Chem.* **2007**, *46*, 7055.
(54) Darmon, J. M.; Stieber, S. C. E.; Sylvester, K. T.; Ferńandez, I.; Lobkovsky, E.; Semproni, S. P.; Bill, E.; Wieghardt, K.; DeBeer, S.; Chirik, P. J. *J. Am. Chem. Soc.* **2012**, *134*, 17125.
(55) Gütlich, P.; Bill, E.; Trautwein, A. *Mössbauer Spectroscopy and Transition Metal Chemistry Fundamentals and Applications*; Springer-Verlag: Berlin, 2011; p 420.
(56) Sur, S. K. *J. Magn. Reson.* **1989**, *82*, 169.
(57) Neese, F. *WIRE Comput. Mol. Sci.* **2012**, *2*, 73.
(58) Bowman, A. C.; Milsmann, C.; Bill, E.; Turner, Z. R.; Lobkovsky, E.; DeBeer, S.; Wieghardt, K.; Chirik, P. J. *J. Am. Chem. Soc.* **2011**, *133*, 17353.
(59) Bowman, A. C.; Milsmann, C.; Bill, E.; Lobkovsky, E.; Weyhermüller, T.; Wieghardt, K.; Chirik, P. J. *Inorg. Chem.* **2010**, *49*, 6110.
(60) Bowman, A. C.; Milsmann, C.; Atienza, C. C. H.; Lobkovsky, E.; Wieghardt, K.; Chirik, P. J. *J. Am. Chem. Soc.* **2010**, *132*, 1676.
(61) Ginsberg, A. P. *J. Am. Chem. Soc.* **1980**, *102*, 111.
(62) Noodleman, L.; Peng, C. Y.; Case, D. A.; Mouesca, J. M. *Coord. Chem. Rev.* **1995**, *144*, 199.
(63) Kirchner, B.; Wennmohs, F.; Ye, S.; Neese, F. *Curr. Opin. Chem. Biol.* **2007**, *11*, 134.
(64) Lu, C. C.; Bill, E.; Weyhermüller, T.; Bothe, E.; Wieghardt, K. *J. Am. Chem. Soc.* **2008**, *130*, 3181.
(65) Bouwkamp, M. W.; Bart, S. C.; Hawrelak, E. J.; Trovitch, R. J.; Lobkovsky, E.; Chirik, P. J. *Chem. Commun.* **2005**, 3408.

(66) Fernandez, I.; Trovitch, R. J.; Lobkovsky, E.; Chirik, P. J. *Organometallics* **2008**, *27*, 109.
(67) Tondreau, A. M.; Atienza, C. C. H.; Darmon, J. M.; Milsmann, C.; Hoyt, H. M.; Weller, K. J.; Nye, S. A.; Lewis, K. M.; Boyer, J.; Delis, J. G. P.; Lobkovsky, E.; Chirik, P. J. *Organometallics* **2012**, *31*, 4886.
(68) Britovsek, G. J. P.; Gibson, V. C.; Spitzmesser, G. K.; Tellmann, K. P.; White, A. J. P.; Williams, D. J. *Dalton Trans.* **2002**, 1159.
(69) Adams, C. J.; Bedford, R. B.; Carter, E.; Gower, N. J.; Haddow, M. F.; Harvery, J. N.; Huwe, M.; Cartes, M. A.; Mansell, S. M.; Mendoza, C.; Murphy, D. M.; Neeve, E. C.; Nunn, J. *J. Am. Chem. Soc.* **2012**, *134*, 10333.
(70) Bedford, R. B.; Carter, E.; Cogswell, P. M.; Gower, N. J.; Haddow, M. F.; Harvey, J. N.; Murphy, D. M.; Neeve, E. C.; Nunn, J. *Angew. Chem., Int. Ed.* **2013**, *52*, 1285.
(71) For selected examples of studies with second and third row transition metals, see: (a) Hoffmann, R.; Yamamoto, A.; Stille, J. K. *Bull. Chem. Soc. Jpn.* **1981**, *54*, 1857. (b) Byers, P. K.; Canty, A. J.; Crespo, M.; Puddephatt, R. J.; Scott, J. D. *Organometallics* **1988**, *7*, 1363. (c) Hill, G. S.; Puddephatt, R. J. *Organometallics* **1998**, *17*, 1478. (d) Crumpton, D. M.; Goldberg, K. I. *J. Am. Chem. Soc.* **2000**, *122*, 962. (e) Williams, B. S.; Goldberg, K. I. *J. Am. Chem. Soc.* **2001**, *123*, 2576. (f) Hartwig, J. F. *Inorg. Chem.* **2007**, *46*, 1936. (g) Ghosh, R.; Emge, T. J.; Krogh-Jespersen, K.; Goldman, A. S. *J. Am. Chem. Soc.* **2008**, *130*, 11317. (h) Racowski, J. M.; Dick, A. R.; Sanford, M. S. *J. Am. Chem. Soc.* **2009**, *131*, 10974.
(72) (a) Grubbs, R. H.; Miyashita, A.; Liu, M.; Burk, P. *J. Am. Chem. Soc.* **1978**, *100*, 2418. (b) Grubbs, R. H.; Miyashita, A.; Liu, M. M.; Burk, P. L. *J. Am. Chem. Soc.* **1977**, *99*, 3863.
(73) Xu, H.; Bernskoetter, W. H. *J. Am. Chem. Soc.* **2011**, *133*, 14956.
(74) (a) Ikariya, T.; Yamamoto, A. *Chem. Lett.* **1976**, 85. (b) Ikariya, T.; Nakamura, Y.; Yamamoto, A. *J. Organomet. Chem.* **1976**, *118*, 101. (c) Yamamoto, A.; Ikariya, T. *J. Organomet. Chem.* **1976**, *120*, 257.
(75) Lau, W.; Huffman; Kochi, J. *Organometallics* **1982**, *1*, 155.
(76) (a) Yamamoto, A.; Morifuji, K.; Ikeda, S.; Saito, T.; Uchida, Y.; Misono, A. *J. Am. Chem. Soc.* **1968**, *90*, 1878. (b) Yamamoto, T.; Yamamoto, A.; Ikeda, S. *Bull. Chem. Soc. Jpn.* **1972**, *45*, 1104.
(77) General considerations and additional experimental details are reported in the Supporting Information.